EFFECTS OF THRESHOLD ON DETECTION PERFORMANCE OF MODIFIED AMPLITUDE-MODULATED JOINT TRANSFORM CORRELATORS

Pitchaya Kaewkasi

A Thesis Submitted in Partial Fulfillment of the Requirements for

the Degree of Doctor of Philosophy in Laser Technology

Suranaree University of Technology

Academic Year 2008

ผลของค่าขีดจำกัดที่มีต่อประสิทธิภาพการตรวจหาโดยจอยท์ทรานส์ฟอร์ม
คอร์รีเลเตอร์แบบผสมคลื่นทางแอมพลิจูดชนิดดัดแปลง

นางพิชญา แก้วกสิ

วิทยานิพนธ์นี้เป็นส่วนหนึ่งของการศึกษาตามหลักสูตรปริญญาวิทยาศาสตรดุษฎีบัณฑิต
สาขาวิชาเทคโนโลยีเลเซอร์
มหาวิทยาลัยเทคโนโลยีสุรนารี
ปีการศึกษา 2551

EFFECTS OF THRESHOLD ON DETECTION PERFORMANCE

OF MODIFIED AMPLITUDE-MODULATED

JOINT TRANSFORM CORRELATORS

Suranaree University of Technology has approved this thesis submitted in partial fulfillment of the requirements for the Degree of Doctor of Philosophy.

Thesis Examining Committee

(Asst. Prof. Dr. Chinorat Kobdaj)

Chairperson

(Prof. Dr. Joewono Widjaja)

Member (Thesis Advisor)

(Prof. Dr. Jun Uozumi)

Member

(Assoc. Prof. Dr. Yupeng Yan)

Member

(Asst. Prof. Dr. Arjuna Chaiyasena)

Member

(Prof. Dr. Pairote Sattayatham)   (Assoc. Prof. Dr. Prapun Manyum)

Vice Rector for Academic Affairs   Dean of Institute of Science

พิชญา แก้วกสิ : ผลของค่าขีดจำกัดที่มีต่อประสิทธิภาพการตรวจหาโดยจอยท์
ทรานส์ฟอร์มคอร์รีเลเตอร์แบบผสมคลื่นทางแอมพลิจูดชนิดดัดแปลง (EFFECTS OF
THRESHOLD ON DETECTION PERFORMANCE OF MODIFIED AMPLITUDE-
MODULATED JOINT TRANSFORM CORRELATORS) อาจารย์ที่ปรึกษา :
ศาสตราจารย์ ดร.ยูโวโน วิดจายา, 92 หน้า.

งานวิทยานิพนธ์นี้นำเสนอการศึกษาผลของค่าขีดจำกัดที่มีต่อการตรวจหาแบบเป้าหมาย
เดี่ยวและหลายเป้าหมาย โดยใช้การจำลองสถานการณ์ด้วยคอมพิวเตอร์ เพื่อเพิ่มประสิทธิภาพของ
จอยท์ทรานส์ฟอร์มคอร์รีเลเตอร์แบบผสมคลื่นทางแอมพลิจูดชนิดดัดแปลง ซึ่งภาพที่ใช้ในการศึกษา
มีสองประเภทที่มีรายละเอียดของภาพ และความเปรียบต่างระหว่างภาพเป้าหมายกับภาพอ้างอิง
แตกต่างกันภายใต้สภาวะที่ภาพเป้าหมายถูกรบกวนด้วยสัญญาณรบกวน ผลการศึกษาจากการ
จำลองสถานการณ์ด้วยคอมพิวเตอร์ พบว่าการเพิ่มประสิทธิภาพการตรวจหาจะต้องทำโดยการเลือก
ใช้ค่าขีดจำกัดที่เหมาะสม ซึ่งขึ้นกับระดับสัญญาณรบกวน, ความเปรียบต่างระหว่างภาพเป้าหมายกับ
ภาพอ้างอิงและรายละเอียดของภาพเป้าหมาย
        เมื่อพิจารณาถึงผลการศึกษาที่ได้จึงได้มีการนำเสนอวิธีการสำหรับปรับปรุงประสิทธิภาพ
การตรวจหาโดยการทำให้ฟิลเตอร์แบบผสมคลื่นทางแอมพลิจูดเรียบ   จากผลการศึกษาพบว่า
การใช้ฟิลเตอร์แบบผสมคลื่นทางแอมพลิจูดแบบเรียบที่ถูกสร้างโดยใช้ค่าขีดจำกัดต่ำเพียงตัวเดียว
จะสามารถเพิ่มประสิทธิภาพได้โดยไม่ต้องคำนึงถึงการตรวจหาเป้าหมาย

สาขาวิชาเทคโนโลยีเลเซอร์และโฟตอนนิกส์   ลายมือชื่อนักศึกษา_____
ปีการศึกษา 2551   ลายมือชื่ออาจารย์ที่ปรึกษา_____
                                                                            ลายมือชื่ออาจารย์ที่ปรึกษาร่วม_____

PITCHAYA KAEWKASI : EFFECTS OF THRESHOLD ON DETECTION
PERFORMANCE OF MODIFIED AMPLITUDE-MODULATED JOINT
TRANSFORM CORRELATORS. THESIS ADVISOR : PROF. JOEWONO
WIDJAJA, Ph.D. 92 PP.

MODIFIED AMPLITUDE-MODULATED JOINT TRANSFORM CORRELATOR/
DETECTION PERFORMANCE

To investigate an optimization performance of a modified amplitude-modulated joint transform correlator, effects of threshold on single- and multiple-target detections are studied using computer simulations. Two types of images with different spatial-frequency contents and contrast are employed as test scenes in the presence of noise in the input plane. The simulation results show that the optimization of the detection performance must be done by selecting appropriate threshold which depends on noise level, contrast and a spatial frequency content of the input target image.

By taking these results into account, a novel method for improving the detection performance by smoothing the amplitude-modulated filter is proposed. As a result, a single smoothed amplitude-modulated filter generated at a low threshold can be used for the optimization performance, regardless of the target detection.

School of Laser Technology and Photonics   Student's Signature_____

Academic Year 2008   Advisor's Signature_____

Co-advisor's Signature_____

ACKNOWLEDGEMENTS

Pitchaya Kaewkasi

CONTENTS

CONTENTS (Continued)

CONTENTS (Continued)

LIST OF TABLES

LIST OF FIGURES

LIST OF FIGURES (Continued)

LIST OF FIGURES (Continued)

LIST OF FIGURES (Continued)

LIST OF FIGURES (Continued)

LIST OF FIGURES (Continued)

LIST OF FIGURES (Continued)

CHAPTER I

INTRODUCTION

1.1 Background

Over the past decades, there are many interests in target detection which is an important process of automatic target recognitions where a target needs to be identified from an input scene or distinguished from a clutter in an image (Khan and Alam, 2005). The target detection can be applied to many real-world applications such as defect, fingerprint, face, and vehicle detections (Antoine, Vandergheynst, Bouyoucef and Murenzi, 1995; Liu, Kim, Lee and Lee, 1998; Mallik and Datta, 1999).

One of interesting methods for performing target detection is joint transform correlator (JTC) (Alam and Karim, 1994; Huang, Lai and Gao, 1997; Widjaja, 1998). Unlike a VanderLugt correlator, the JTC does not require a synthesis of complex matched filters and stringent alignment (Goodman, 1996). This method is implemented by performing a correlation between an input target and reference images. A similarity between these two images can be measured by quantifying height and sharpness of a correlation output signal. If the target image is identical to the reference image, its correlation output has a high and sharp peak. In the case of non-identical images, its correlation peak is low and broad.

However, an implementation of the JTC has several limitations, such that it produces a strong zero-order peak with a broad correlation width in a correlation output and that its discrimination ability is low. These problems cause difficulties in correctly identifying objects in automatic target detections (Alam and Karim, 1993).

Therefore, there are many research devoted to improving the detection performance of the JTC. Amplitude-modulated JTC (AMJTC) is one of several approaches to eliminate the problems of the classical JTC and is performed by multiplying a joint power spectrum (JPS) with an amplitude-modulated filter (AMF) whose transfer function is determined by thresholding the power spectrum of the reference image (Feng, Zhao and Xia, 1991). Although this method produces a better correlation result than the classical JTC, it is not tolerant to the presence of noise. To obviate this problem, Huang *et al.* (Huang, Lai and Gao, 1997) proposed a method for improving the performance of the AMJTC which is called the modified AMJTC. This is performed by subtracting the power spectra of the reference and of the target images from the JPS before multiplying with the AMF. Consequently, the correlation performance of this approach is enhanced and thus it is better than those of other JTC approaches.

1.2 Significance of study

The modified AMJTC is a useful method for eliminating the limitations of the classical JTC and to improve simultaneously the performance of the AMJTC. It is a fact that an effectiveness of the modified AMJTC depends on the selected threshold value of the AMF. Nevertheless, the criteria for selecting the appropriate threshold has not been fully investigated. Accordingly, it is important to study the effects of the threshold on target detection by using the modified AMJTC. On the basis of the resultant study, a further improvement of the modified AMJTC is proposed.

1.3 Research objectives

The objectives of this research are first to study quantitatively the effects of threshold on detection performance of the modified AMJTC. The second is to improve further the detection performance.

1.4 Scope and limitations of the study

This dissertation studies the effects of threshold on the performance of the single- and multiple-target detections of the modified AMJTC and improves the performance of the AMF by using computer simulation. The scope and limitations of the study are described as follows.

1.4.1 Target of interest

Two types of images with different spatial frequency contents are used as test scenes in the presence of noise in the input plane and a contrast difference between the target and the reference images that may arise from unbalanced illumination.

1.4.2 Performance metrics

The metrics used for measuring the detection performance of the modified AMJTC are correlation peak intensity (CP), full area at half-maximum (FAHM) of the correlation peak, the ratio of peak to the correlation deviation (PCD) (Roberge and Sheng, 1994), and the primary to the secondary peaks ratio (PSR) (Widjaja and Suripon, 2005).

For the purpose of studying the effects of the threshold on target detection, the research procedure shown in Fig. 1 is followed. Firstly, the image of interest is prepared and duplicated into the target and the reference images. Secondly, the noise-free and the noisy images are generated from the target. Next, the target and reference images are formed as the joint input image of the modified AMJTC. After computing

digitally the modified AMJTC, the CP, the FAHM, the normalized PCD or the PSR of the correlation output are quantitatively measured.

```
                    ┌─────────────────┐
                    │ Generate images │
                    └─────────────────┘

   ┌─────────────────┐              ┌─────────────────┐
   │    Original     │              │    Original     │
   │  target images  │              │ reference images│
   └─────────────────┘              └─────────────────┘
         Noise-free target

 ┌──────────────┐
 │  Add noise:  │
 │ Noisy target │
 └──────────────┘
              ┌──────────────────────────┐
              │  Perform modified AMJTC   │
              │   by computer simulation  │
              └──────────────────────────┘

    ┌──────────────────────────────────────────────┐
    │ Measure CP, FAHM, Normalized PCD or PSR        │
    └──────────────────────────────────────────────┘
```
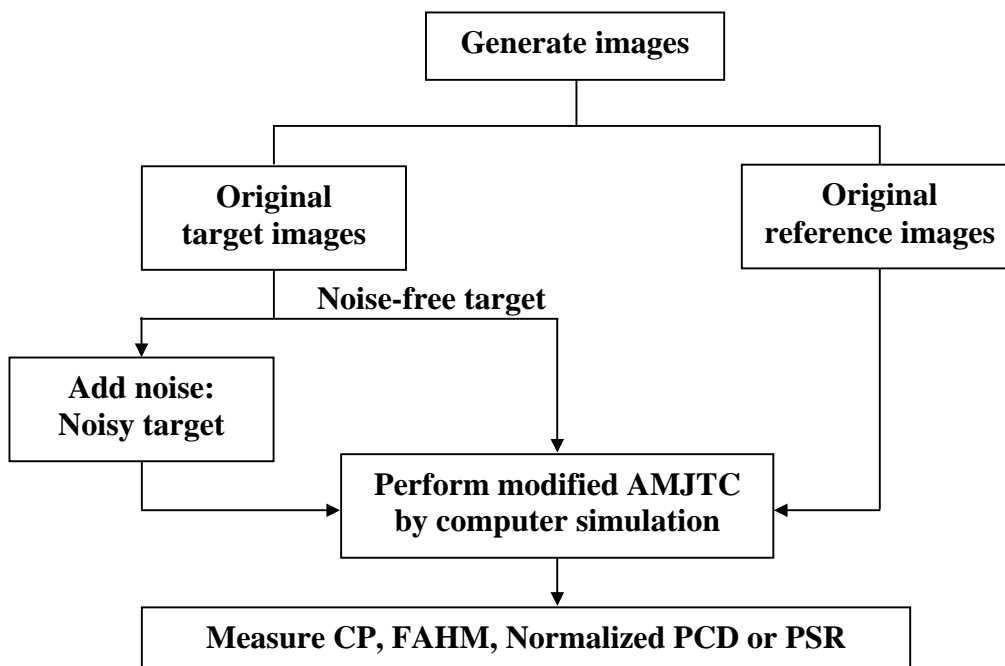
Figure 1.1 Diagram of research procedure.

The simulation is performed by using Matlab 6.0 run on a Windows-based personal computer. The FFT2 and the IMNOISE commands are used to calculate the two-dimensional Fourier spectrum of the images and to add the Gaussian noise to an image, respectively.

1.5 Organization

This dissertation consists of six chapters. This is the first chapter which provides a brief background and introduction of the dissertation. The principles of the JTC and the modified AMJTC are described in the Chapter II. Chapter III discusses the study of single-target detection using modified AMJTC. The study of multiple-target detection is presented in the Chapter IV. Subsequently, the improvement of the

modified AMJTC is discussed in Chapter V. Finally, Chapter VI provides the conclusions of this dissertation.

CHAPTER II

MODIFIED AMPLITUDE-MODULATED

JOINT TRANSFORM CORRELATION

In the past few years, the JTC has been widely used for implementing real-time optical pattern recognition (Alam and Karim, 1994; Huang, Lai and Gao, 1997; Widjaja, 1998). This is because unlike the VanderLugt correlator, a priori synthesis of complex matched filters and stringent alignment of filters are not necessary in the JTC (Goodman, 1996). By taking this advantage into account, real-time implementation of the JTC can be accomplished by using a spatial light modulator (SLM) together with a charge-coupled device (CCD) sensor. This architecture is very useful for pattern recognition. However, the JTC suffers inherently from several limitations such that it produces a strong zero-order peak with a broad correlation width in a correlation output and that its discrimination ability is low. These problems cause difficulties in correctly identifying objects in automatic target detections (Alam and Karim, 1993). Therefore, an improvement of its detection performance is of particular interest.

Amplitude-modulated JTC (AMJTC) is one of methods for overcoming the limitations of the classical JTC (Feng, Zhao and Xia, 1991). Although this method produces a better correlation result than the classical JTC, it is not tolerant to the presence of noise. Consequently, Huang *et al.* (Huang, Lai and Gao, 1997) have proposed a method for improving the performance of the AMJTC which is called the modified AMJTC.

In this chapter, the standard architecture of the JTC is reviewed in Sect. 2.1. Next, the theory of the modified AMJTC is provided in Sect. 2.2.

2.1 Joint transform correlation

A schematic diagram for implementing the JTC is shown in Fig. 2.1 which constitutes from two-step process. The first step is to generate the JPS by performing an optical Fourier transform of the reference and the target images and recording their power spectra onto a photographic film. The second one is to generate a cross-correlation operation. After development process, the developed film is placed at the input plane. The optical Fourier transform of the recorded JPS gives the correlation output.
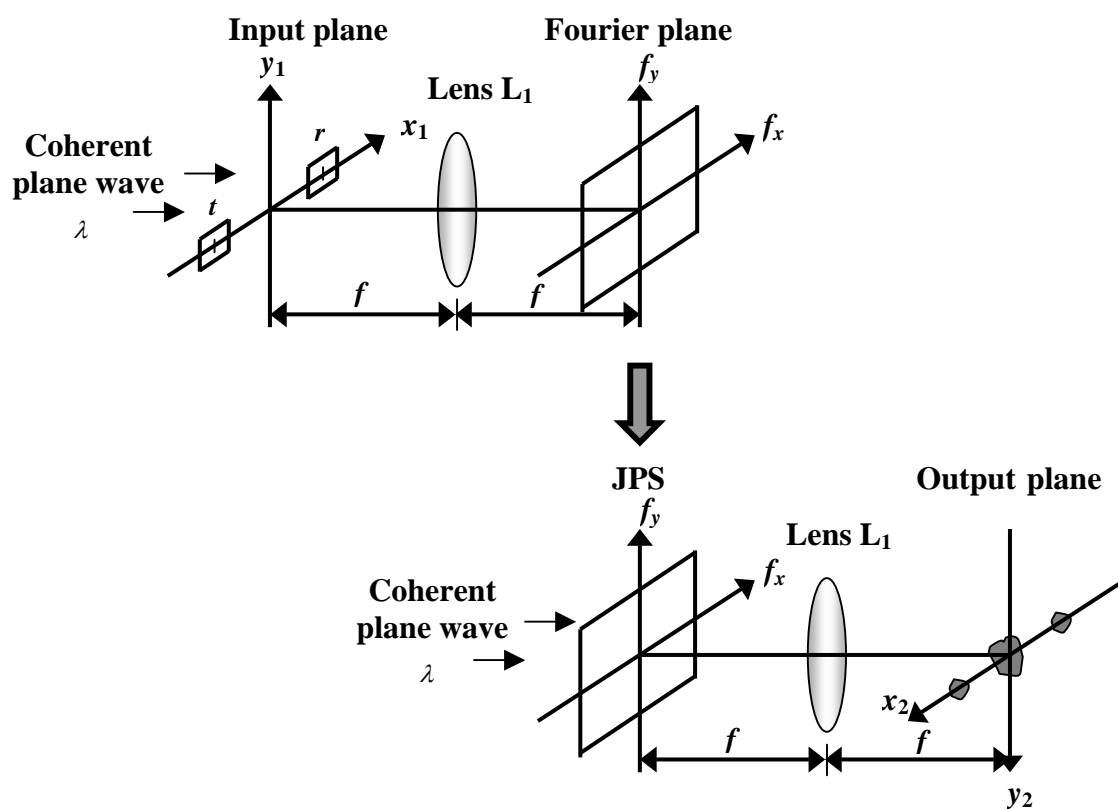
Figure 2.1 Schematic diagram for implementing joint transform correlation.

As shown in Fig. 2.1, a joint input image consists of the reference image $r(x_1, y_1)$ and the input target image $t(x_1, y_1)$ that are placed side-by-side on the input plane with a separation of $2x_0$. In the presence of noise in the input, the joint input image can be mathematically expressed as

$$f(x_1, y_1) = r(x_1 - x_0, y_1) + t(x_1 + x_0, y_1) + n(x_1 + x_0, y_1), \qquad (2.1)$$

where $n(x_1, y_1)$ is the additive Gaussian noise in the input. By illuminating perpendicularly the input plane with a coherent plane wave having a wavelength λ, the joint Fourier spectrum is generated at the back of the lens. The generated JPS at the Fourier plane is mathematically given by

$$
\begin{aligned}
|F(f_x, f_y)|^2 = & |R(f_x, f_y)|^2 + |T(f_x, f_y)|^2 + |N(f_x, f_y)|^2 \\
& + T^*(f_x, f_y)N(f_x, f_y) + T(f_x, f_y)N^*(f_x, f_y) \\
& + R(f_x, f_y)T^*(f_x, f_y)\exp(-j4\pi f_x x_0) \\
& + R^*(f_x, f_y)T(f_x, f_y)\exp(j4\pi f_x x_0) \\
& + R(f_x, f_y)N^*(f_x, f_y)\exp(-j4\pi f_x x_0) \\
& + R^*(f_x, f_y)N(f_x, f_y)\exp(j4\pi f_x x_0).
\end{aligned}
\qquad (2.2)
$$

Here $R(f_x, f_y)$, $T(f_x, f_y)$ and $N(f_x, f_y)$ are the Fourier transforms of the reference, the target and the noise, respectively. f_x and f_y stand for the spatial-frequency coordinates in the horizontal and the vertical directions at the Fourier plane, respectively. They are associated with the actual coordinates (x, y) by $x = \lambda f f_x$ and $y = \lambda f f_y$ with f stands for the focal length of the lens L_1. By performing optically Fourier transform of the recorded JPS, the correlation result in the output plane is obtained as

$$c\left(x_2, y_2\right) = r(x_2, y_2) * r(x_2, y_2) + t(x_2, y_2) * t(x_2, y_2)$$
$$+ n(x_2, y_2) * n(x_2, y_2) + t(x_2, y_2) * n(x_2, y_2)$$
$$+ r(x_2, y_2) * t(x_2, y_2) \otimes \delta(x_2 - 2x_0, y_2)$$
$$+ r(x_2, y_2) * t(x_2, y_2) \otimes \delta(x_2 + 2x_0, y_2)$$
$$+ r(x_2, y_2) * n(x_2, y_2) \otimes \delta(x_2 - 2x_0, y_2)$$
$$+ r(x_2, y_2) * n(x_2, y_2) \otimes \delta(x_2 + 2x_0, y_2), \qquad (2.3)$$

where $\otimes$ and $*$ denote the convolution and the correlation operations, respectively. In Eq. (2.3), the first three terms correspond to the autocorrelations of the reference, the target and the noise, respectively. The fourth term is the cross-correlation between the target and the noise. The last four terms produce the desired cross-correlations between the reference and the target which are located at the location $x_2 = 2x_0$ and $x_2 = -2x_0$, respectively. They are corrupted by the correlation terms of noise.

2.2 Modified amplitude-modulated joint transform correlation

Figure 2.2 illustrates a schematic diagram of an optical setup for implementing the real-time modified AMJTC. The architecture of this setup is based on an optical Fourier transform where an electronically addressed SLM (EASLM), placed in the front focal plane of the Fourier transforming lens L1, is used to display an input image to be processed. The CCD1 placed at the back focal plane of the lens is used to capture its Fourier transformed output. In this setup, a set of reference images and their corresponding power spectra are prepared and stored into a computer system prior to detection. The power spectrum is optically generated by taking the Fourier transform of the reference image displayed onto the EASLM. The generated power spectrum at the back focal plane of the lens is captured by the CCD1 and stored into the computer system. In order to detect the target image $t(x_1, y_1)$, the input scene is captured by using the CCD2. After storing the captured target image into the

computer, its power spectrum is generated and stored in the same way as the reference image. Subsequently, the reference $r(x_1, y_1)$ and the target $t(x_1, y_1)$ corrupted by noise $n(x_1, y_1)$ are displayed side-by-side on the EASLM with a separation of $2x_0$ to form the joint input image. By illuminating perpendicularly the EASLM placed in the front focal plane of a lens L1 with a coherent plane wave, the joint Fourier spectrum is generated at the back of the lens L1. Capturing the intensity of this spectrum by using CCD1 yields the JPS.
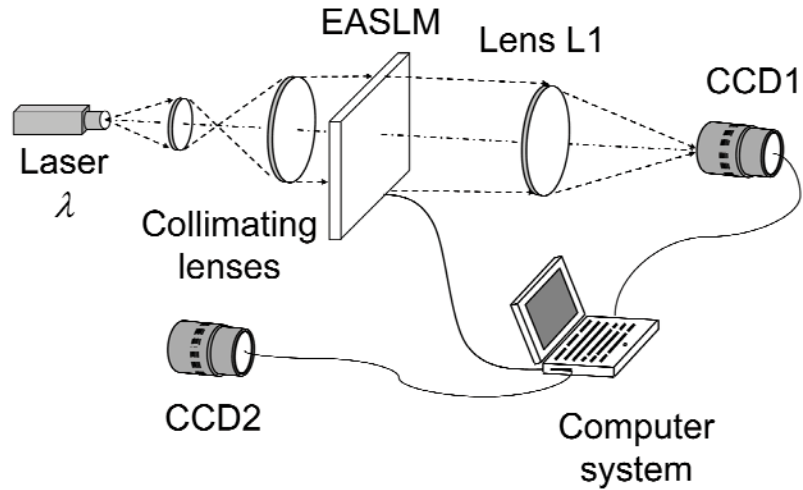
Figure 2.2 Schematic diagram of optical setup for implementing the real-time
modified AMJTC.

To overcome the problems of a complicated strong zero-order and the noise terms, the power spectra of the reference and of the noise-corrupted input target that correspond to the first five terms of Eq. (2.2) are subtracted from Eq. (2.2) (Huang, Lai and Gao, 1997). The subtraction yields

$$U(f_x, f_y) = |F(f_x, f_y)|^2 - \{|R(f_x, f_y)|^2 + |T(f_x, f_y)|^2 + |N(f_x, f_y)|^2$$
$$+ T^*(f_x, f_y)N(f_x, f_y) + T(f_x, f_y)N^*(f_x, f_y)\}$$

$$= R(f_x, f_y)T^*(f_x, f_y)\exp(-j4\pi f_x x_0)$$
$$+ R^*(f_x, f_y)T(f_x, f_y)\exp(j4\pi f_x x_0)$$
$$+ R(f_x, f_y)N^*(f_x, f_y)\exp(-j4\pi f_x x_0)$$
$$+ R^*(f_x, f_y)N(f_x, f_y)\exp(j4\pi f_x x_0). \tag{2.4}$$

As can be seen from Eq. (2.4), the dc and some noise terms are eliminated. This increases robustness of the JTC to noise.

To enhance a discrimination ability of the JTC, the resultant JPS is modulated by the AMF defined as

$$H_{AMF}(f_x, f_y) = \begin{cases} \text{TH}\big/ |R(f_x, f_y)|^2 & \text{when } |R(f_x, f_y)|^2 \geq \text{TH} \\ 1 & \text{when } |R(f_x, f_y)|^2 < \text{TH}, \end{cases} \tag{2.5}$$

where TH is the threshold value used to determine the transfer function of the AMF. Since for a given threshold value TH the second condition of Eq. (2.5) can be satisfied by several frequency components of the reference image, the synthesized AMF may contain several cutoff frequencies. Therefore, the transfer function of the AMF is not a smooth function. Below the cutoff frequency, the frequency component of the input signal is attenuated by a factor $\text{TH}\big/ |R(f_x, f_y)|^2$, while the higher ones are not affected. In comparison with low threshold value, the AMF synthesized by using the high threshold value attenuates a narrow band of low frequency components around the origin. When the threshold value becomes lower, the attenuation extends to wider band of frequency components. Therefore, for a low threshold, only high frequency components can pass the filter without attenuation. These characteristics can be understood from the following figures. Figure 2.3 shows the 1-D scan of the power spectra of a fingerprint image, while its AMFs generated by the low and the high threshold values are illustrated in Figs. 2.4 and 2.5, respectively. Both transfer functions oscillate as the spatial frequencies increase, yielding many passbands. In

comparison with Fig. 2.4, the transfer function of Fig. 2.5 contains smaller number of passbands. Therefore, only a narrow set of low frequency components of the resultant JPS is suppressed. In contrast, the use of low threshold causes broader suppression of frequency components. Figures 2.6 and 2.7 show the 3-D plot and 1-D scan of the low and the high threshold values, respectively.
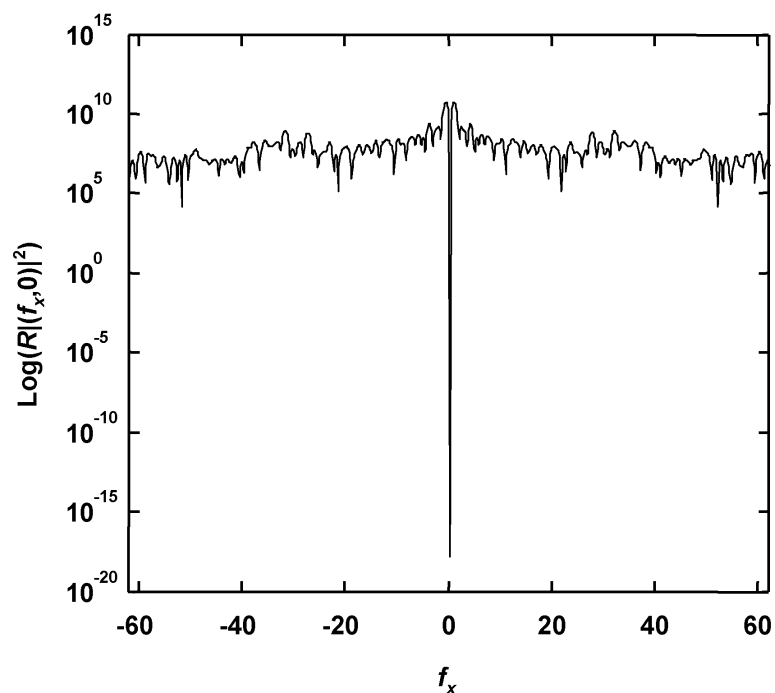
Figure 2.3 The 1-D scan of the power spectrum of a fingerprint image.

(a)

(b)
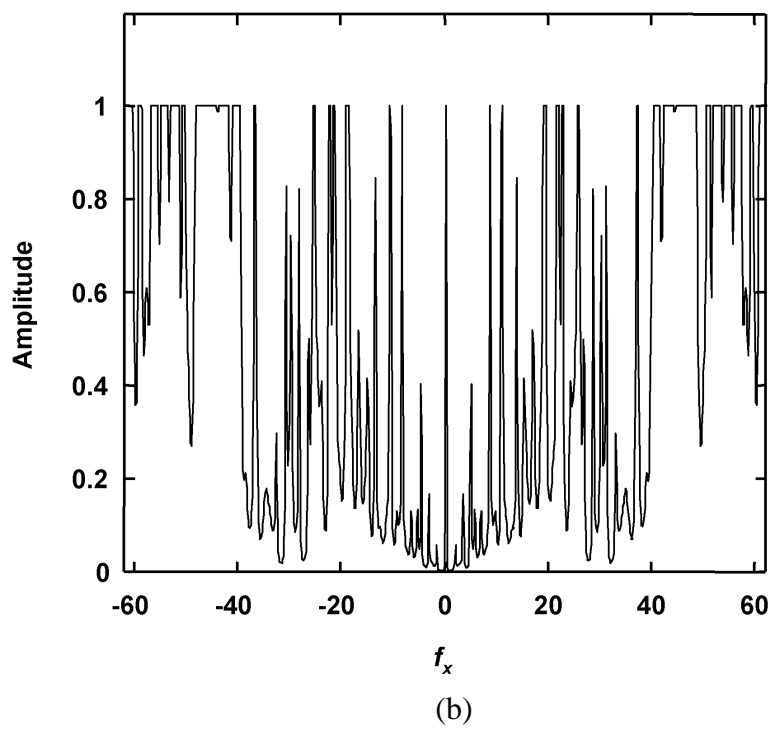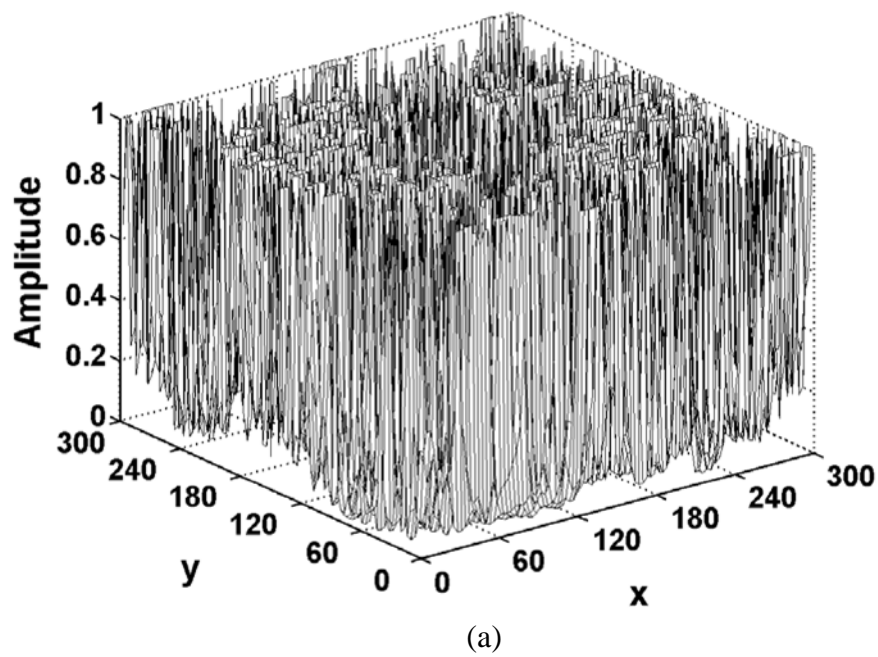
Figure 2.4 (a) 3-D plot and (b) 1-D scan of AMF of fingerprint generated by the low

threshold.

(a)

(b)
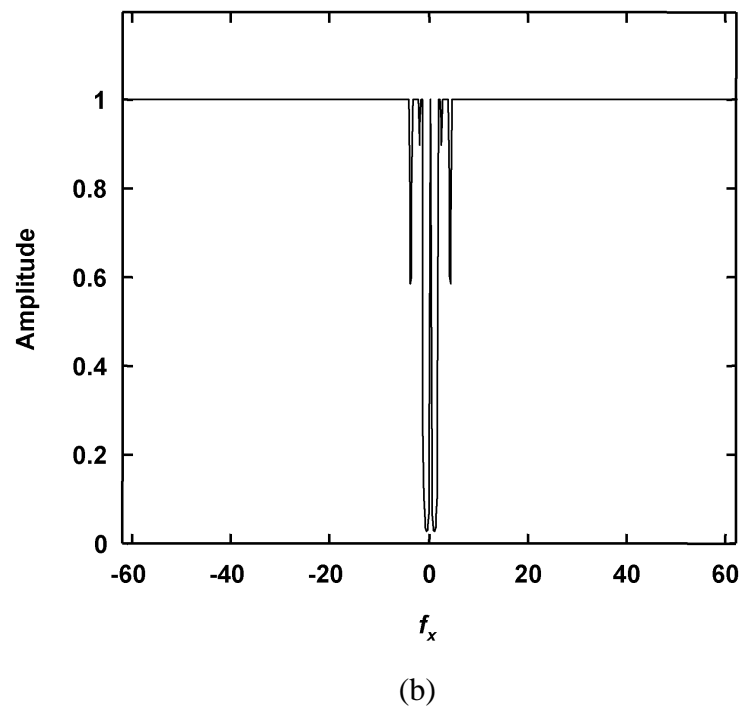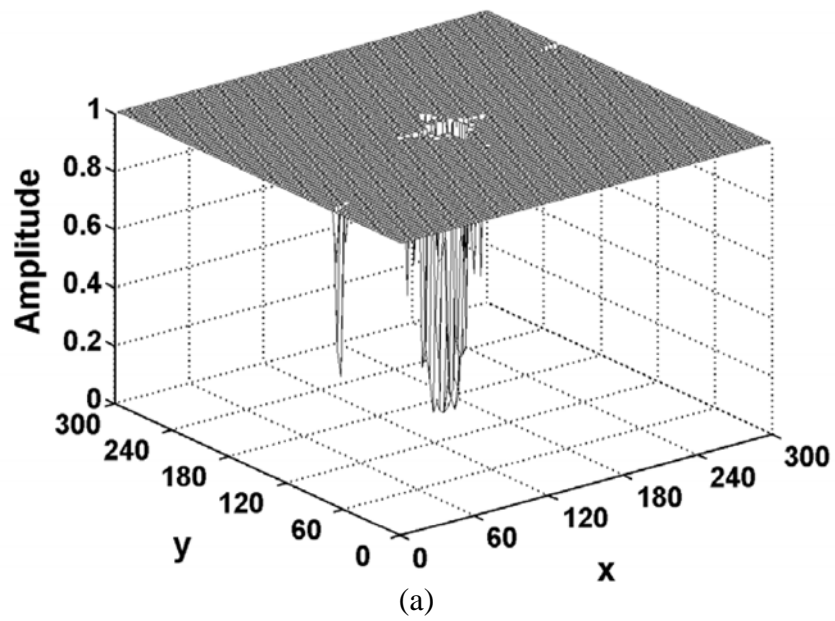
Figure 2.5 (a) 3-D plot and (b) 1-D scan of AMF of fingerprint generated by the high

threshold.

15

(a)

f_x

(b)
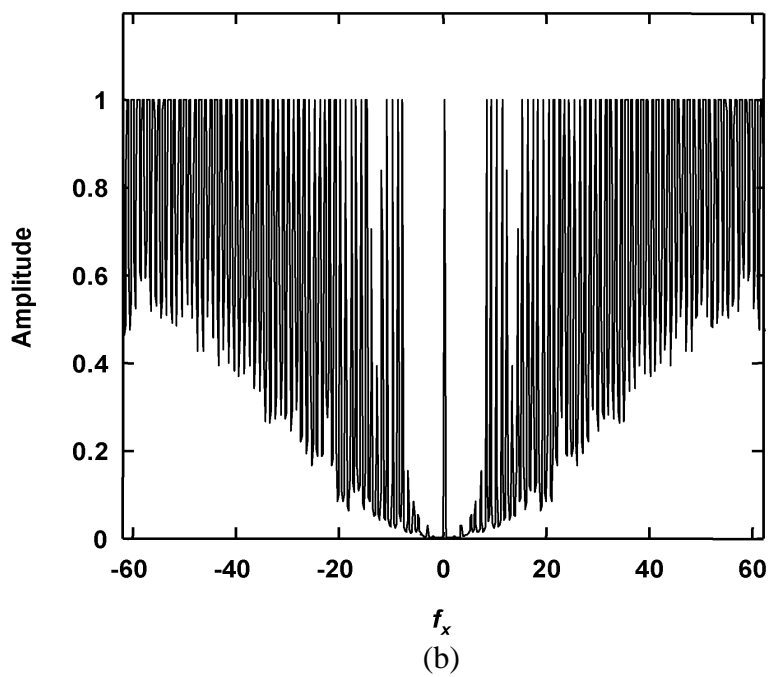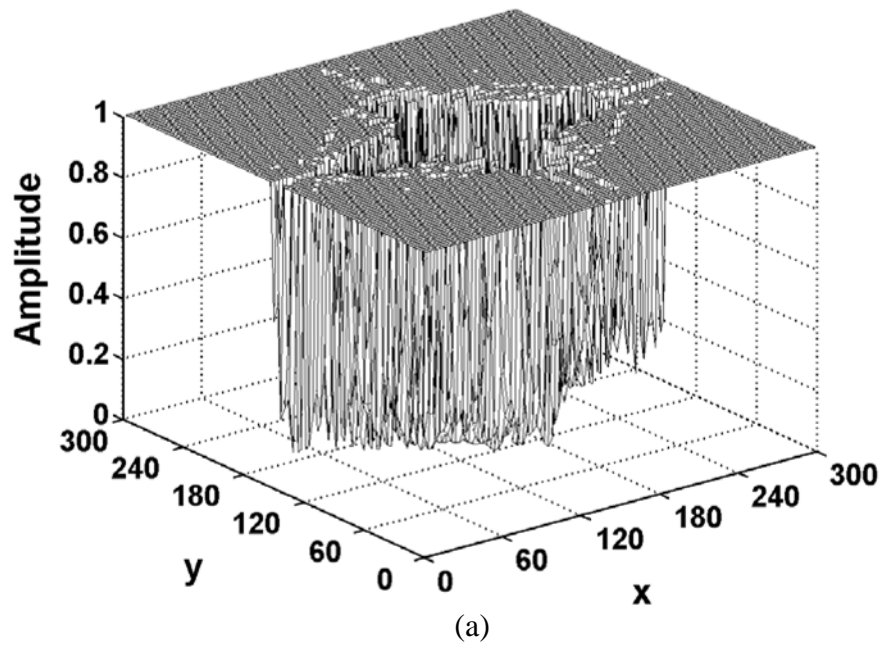
Figure 2.6 (a) 3-D plot and (b) 1-D scan of AMF of human face generated by the low

threshold.

(a)

(b)
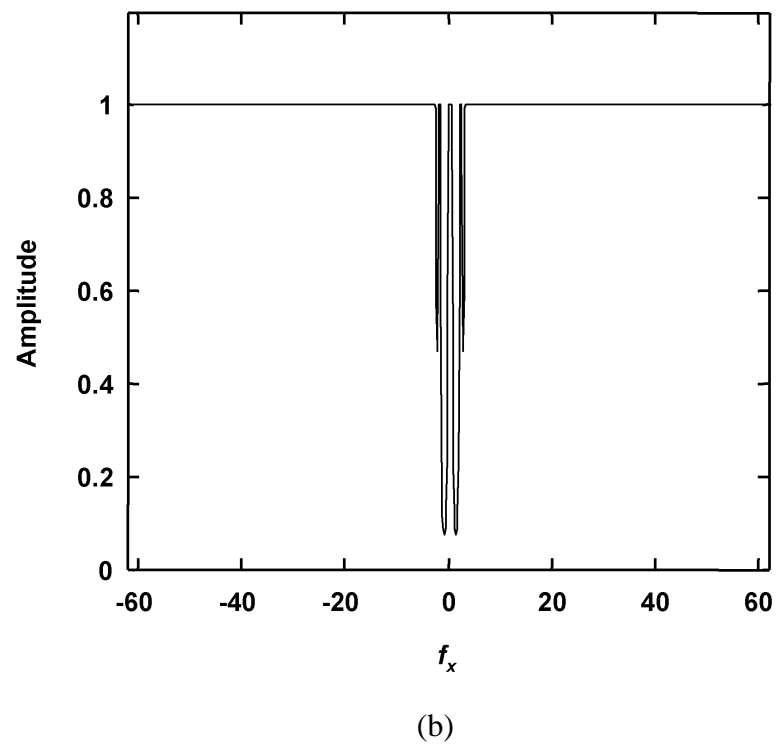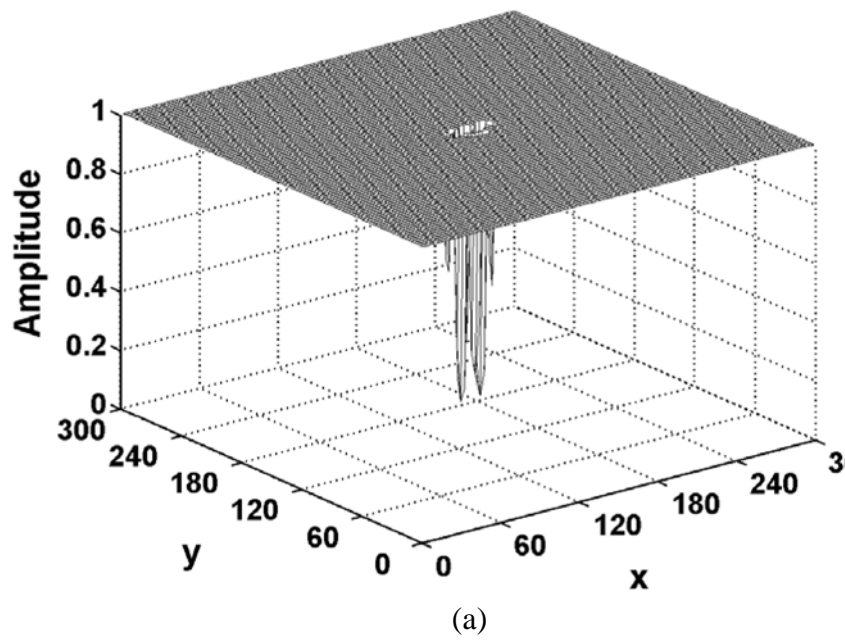
Figure 2.7   (a) 3-D plot and (b) 1-D scan of AMF of human face generated by the

high threshold.

The modified amplitude modulated JPS can be mathematically rewritten as

$$H_{\text{AMF}}(f_x, f_y)U(f_x, f_y) = H_{\text{AMF}}(f_x, f_y)\{R(f_x, f_y)T^*(f_x, f_y)\exp(-j4\pi f_x x_0)$$
$$+ T(f_x, f_y)R^*(f_x, f_y)\exp(j4\pi f_x x_0)$$
$$+ R(f_x, f_y)N^*(f_x, f_y)\exp(-j4\pi f_x x_0)$$
$$+ N(f_x, f_y)R^*(f_x, f_y)\exp(j4\pi f_x x_0)\}. \tag{2.6}$$

By taking the property of the AMF into account, Eq. (2.6) can be mathematically regarded as a process of attenuating the spectrum components of the modified JPS below the cutoff frequency of the AMF by the factor $\text{TH}/|R(f_x, f_y)|^2$. Since the higher frequency spectrum is not affected, this is equivalent to an edge enhancement process.

Finally, by displaying the modified JPS into the EASLM, the optical Fourier transform produces the correlation output

$$c(x, y) = \mathcal{F}^{-1}\{H_{\text{AMF}}(f_x, f_y)U(f_x, f_y)\}$$
$$= h_{\text{AMF}}(x, y) \otimes r(x, y) * t(x, y) \otimes \{\delta(x - 2x_0, y) + \delta(x + 2x_0, y)\}$$
$$+ h_{\text{AMF}}(x, y) \otimes r(x, y) * n(x, y) \otimes \{\delta(x - 2x_0, y) + \delta(x + 2x_0, y)\}, \tag{2.7}$$

where $\mathcal{F}^{-1}$ denotes the inverse Fourier transform operator and $h_{\text{AMF}}(x, y)$ corresponds to the impulse response of the AMF. The first term of Eq. (2.7) is the correlation between the reference and the target, while the second one is the correlation between the reference and the noise. Both terms are convolved with the impulse response $h_{\text{AMF}}(x, y)$. These pairs of correlation appear at the position $\pm 2x_0$. When the threshold value of the AMF is properly selected, the noise will be lowered and the correlation width will be sharpened.

CHAPTER III

EFFECTS OF THRESHOLD ON SINGLE-TARGET

DETECTION

In this chapter, the effect of threshold on the single-target detection using the modified AMJTC is studied by means of computer simulation. Fingerprint and human face images are used as test scenes having high- and low-spatial-frequency contents. Since in practice the input scenes are captured from the outside world by using CCD image sensors, they are far from ideal. To conform to this condition, besides adding the Gaussian noise the contrast of the input scenes are set to be different from the reference images, because of unbalanced illumination.

3.1 Detection of noisy target with different contrast

By taking the contrast difference into account, Eq. (2.1) can be mathematically rewritten as

$$f(x_1, y_1) = r(x_1 - x_0, y_1) + c_T t(x_1 + x_0, y_1) + n(x_1 + x_0, y_1), \qquad (3.1)$$

where c_T is the ratio of the amplitude of the target image to the reference image. The factor c_T is greater than, equal to, or smaller than 1 when the contrast of the reference image is lower than, equal to, or higher than that of the target, respectively. After Fourier transforming the joint input image by lens L1 shown in Fig. 2.1, its JPS can be express as

$$|F(f_x, f_y)|^2 = |R(f_x, f_y)|^2 + c_T^2 |T(f_x, f_y)|^2 + |N(f_x, f_y)|^2$$
$$+ c_T \left[T^*(f_x, f_y) N(f_x, f_y) + T(f_x, f_y) N^*(f_x, f_y) \right]$$
$$+ c_T \left[R(f_x, f_y) T^*(f_x, f_y) \exp(-j4\pi f_x x_0) \right.$$
$$\left. + R^*(f_x, f_y) T(f_x, f_y) \exp(j4\pi f_x x_0) \right]$$
$$+ R(f_x, f_y) N^*(f_x, f_y) \exp(-j4\pi f_x x_0)$$
$$+ R^*(f_x, f_y) N(f_x, f_y) \exp(j4\pi f_x x_0). \tag{3.2}$$

By subtracting the power spectra of the reference and of the noise-corrupted target images from the JPS, the result of the subtraction becomes

$$U(f_x, f_y) = |F(f_x, f_y)|^2 - \left\{ |R(f_x, f_y)|^2 + c_T^2 |T(f_x, f_y)|^2 + |N(f_x, f_y)|^2 \right.$$
$$\left. + c_T \left[T^*(f_x, f_y) N(f_x, f_y) + T(f_x, f_y) N^*(f_x, f_y) \right] \right\}$$
$$= c_T \left[R(f_x, f_y) T^*(f_x, f_y) \exp(-j4\pi f_x x_0) \right.$$
$$\left. + R^*(f_x, f_y) T(f_x, f_y) \exp(j4\pi f_x x_0) \right]$$
$$+ R(f_x, f_y) N^*(f_x, f_y) \exp(-j4\pi f_x x_0)$$
$$+ R^*(f_x, f_y) N(f_x, f_y) \exp(j4\pi f_x x_0). \tag{3.3}$$

The resultant JPS is then multiplied by the AMF which is defined in Eq. (2.5). The modified JPS is rewritten as

$$H_{\text{AMF}}(f_x, f_y) U(f_x, f_y) = H_{\text{AMF}}(f_x, f_y) \left\{ c_T \left[R(f_x, f_y) T^*(f_x, f_y) \exp(-j4\pi f_x x_0) \right. \right.$$
$$\left. + R^*(f_x, f_y) T(f_x, f_y) \exp(j4\pi f_x x_0) \right]$$
$$+ R(f_x, f_y) N^*(f_x, f_y) \exp(-j4\pi f_x x_0)$$
$$\left. + R^*(f_x, f_y) N(f_x, f_y) \exp(j4\pi f_x x_0) \right\}. \tag{3.4}$$

The Fourier transformation of the modified JPS gives the correlation output

$$c(x, y) = \mathcal{F}^{-1} \left\{ H_{\text{AMF}}(f_x, f_y) U(f_x, f_y) \right\}$$
$$= c_T h_{\text{AMF}}(x, y) \otimes r(x, y) * t(x, y) \otimes \left\{ \delta(x - 2x_0, y) + \delta(x + 2x_0, y) \right\}$$
$$+ h_{\text{AMF}}(x, y) \otimes r(x, y) * n(x, y) \otimes \left\{ \delta(x - 2x_0, y) + \delta(x + 2x_0, y) \right\}. \tag{3.5}$$

Equation (3.5) shows that besides being corrupted by the noise, the first term of Eq. (3.5) which gives the enhanced correlation between the reference and the target is scaled by the contrast ratio.

3.2 Computer simulation

Figures 3.1(a) and 3.1(b) show the original high-contrast test scenes, while their low-contrast images are illustrated in Figs. 3.1(c) and 3.1(d). The fingerprint and the human face images consisted of 124×186 pixels with 8-bit gray levels. They were prepared and duplicated as the target and the reference images. The IMNOISE command of the Matlab was used to generate the additive Gaussian noise of the target images.

(a)   (b)

(c)   (d)
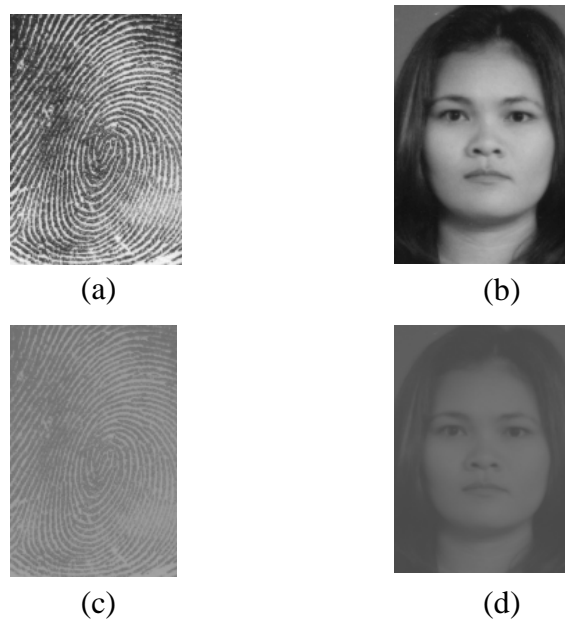
Figure 3.1 Original test images: (a) high-contrast fingerprint, (b) high-contrast human face, (c) low-contrast fingerprint, and (d) low-contrast human face.

The contrast of the two images were measured by using the contrast function defined as (Hess, Bradley and Piotrowski, 1983)

$$C(u,v) = \frac{2A(u,v)}{DC},$$ (3.6)

where $A(u,v)$ is the amplitude of the power spectrum of the image. The average contrast functions of the test images were 0.28×10^{-2} and 0.11×10^{-2} for Figs. 3.1(a) and 3.1(b), respectively. They were 0.29×10^{-3} and 0.70×10^{-3} for the low-contrast images shown in Figs. 3.1(c) and 3.1(d), respectively.

```
                    ┌──────────────┐
                    │    Start     │
                    └──────────────┘
                           │
         ┌─────────────────────────────────┐
         │   Generate the joint input image │
         └─────────────────────────────────┘
                           │
         ┌─────────────────────────────────┐
         │    Compute its Fourier spectrum  │
         └─────────────────────────────────┘
                           │
         ┌─────────────────────────────────┐
         │    Compute the modulus square    │
         └─────────────────────────────────┘
                           │
         ┌─────────────────────────────────┐
         │  Subtract with the power spectra │
         │  of the target and of the reference │
         │             images               │
         └─────────────────────────────────┘
                           │
         ┌─────────────────────────────────┐
         │        Multiply with AMF         │
         └─────────────────────────────────┘
                           │
         ┌─────────────────────────────────┐
         │  Compute the inverse Fourier     │
         │            transform             │
         └─────────────────────────────────┘
                           │
         ┌─────────────────────────────────┐
         │    Compute the modulus square    │
         └─────────────────────────────────┘
                           │
         ┌─────────────────────────────────┐
         │    Measure CP, FAHM, PCD         │
         └─────────────────────────────────┘
                           │
                    ┌──────────────┐
                    │    Stop      │
                    └──────────────┘
```
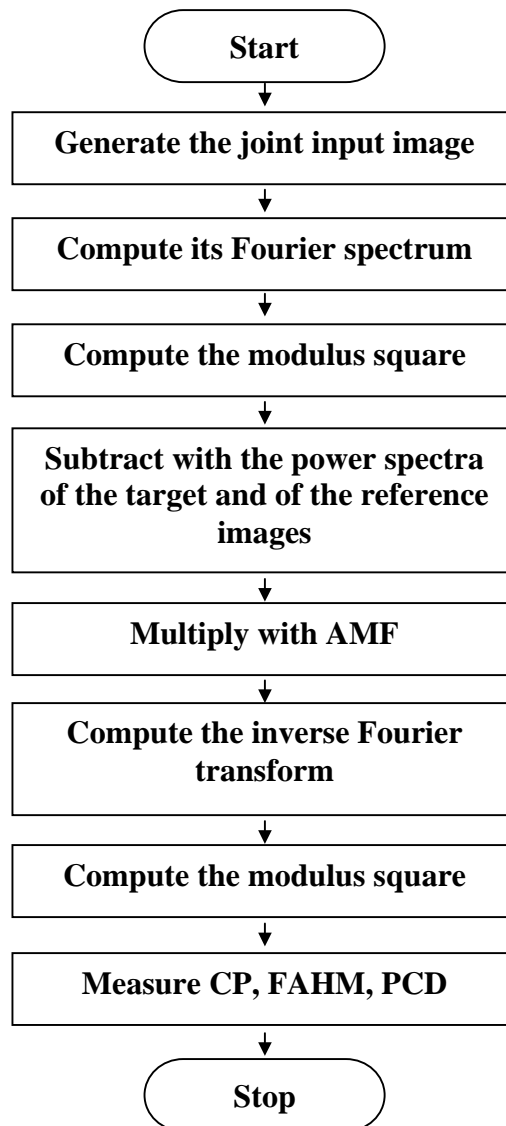
Figure 3.2 Flowchart for simulating the operation of the modified AMJTC.

Figure 3.2 illustrates a flowchart for simulating the modified AMJTC. The joint input image was composed of the reference and the target images displayed side-by-side in the area of 832×624 pixels with the separation of $2x_0 = 248$ pixels. By calculating its Fourier transform and then taking the modulus squared of the resultant spectrum, the JPS was obtained. This Fourier transform operation was performed by using the FFT2 command. Next, the power spectra of the reference and the target images were subtracted from the JPS. Its resultant was modulated by the AMF generated in the following steps:

- A moving average of the power spectrum of the reference image was computed.

- From the averaged spectrum, several points separated by equal interval were selected between the zero and the highest spatial frequencies along one of the axis of the power spectrum.

- The value of the power spectrum at each selected point was used as the threshold value to generate the corresponding AMF.

By calculating the Fourier transform of the modified amplitude-modulated JPS and taking the modulus squared of the result, the correlation output intensity was obtained. Finally, the correlation output quality was quantitatively measured by means of the CP, the FAHM, and the PCD. The PCD is mathematically defined as (Roberge and Sheng, 1994)

$$\text{PCD} = \frac{I(i,j)_{\max}}{\left\{ \frac{1}{K \times L} \sum_{i=0}^{K-1} \sum_{j=0}^{L-1} \left[I(i,j) - E\{I(i,j)\} \right]^2 \right\}^{1/2}}, \qquad (3.7)$$

where $I(i,j)_{\max}$ is the maximum intensity of the correlation output and $E\{I(i,j)\}$ is

the mean of the correlation intensity. When the target matches with the reference, the PCD is large, because the correlation output is sharp and its standard deviation (SD) is small. However, when the target does not match with the reference, the PCD is small because the correlation output is broad and its standard deviation is large. In order to compare with the detection performance of the classical JTC, the PCD obtained from the modified AMJTC was normalized by the PCD of the classical JTC. It is expected that the normalized PCD will be greater than 1, because the performance of the modified AMJTC is better than that of the classical JTC.

In order to obtain results applicable to more general images, the threshold value is related to the percentage number of pixels of the power spectrum having value less than the threshold defined as

$$N = \frac{\text{Number of pixels with value less than the threshold value}}{\text{Total number of pixels of the power spectrum}}. \tag{3.8}$$

According to Eq. (2.5), the pixels of the power spectrum with value less than the selected threshold value correspond to the pixel of the AMF having a unit amplitude. Hence, Eq. (3.8) can be rewritten as

$$N = \frac{\text{Number of pixels of the AMF with value 1}}{\text{Total number of pixels of the AMF}}. \tag{3.9}$$

Since, high and low values of the percentage N can be associated with the AMF generated by using high and low threshold values, respectively, the percentage N represents the extent of attenuation of the modified JPS. When the percentage N is high, the attenuation occurs in narrow band of low-spatial frequencies, while lower value affects wider band of spatial frequencies.

3.3 Simulation results

3.3.1 High-contrast fingerprint as the reference image

The 3-D plots of the autocorrelation of the noise-free high-contrast fingerprints which were pre-processed by using the AMF with $N = 64.7\%$ that corresponds to low threshold and $N = 99.8\%$ that corresponds to high threshold are shown in Figs. 3.3(a) and 3.3(b), respectively. Their correlation peaks are sharp with the FAHMs always equal to 1×1 pixel. However, it can be seen that the correlation peak intensity of Fig. 3.3(a) is about two orders of magnitude lower than that of Fig. 3.3(b), because the AMF with low threshold value eliminates the low-spatial-frequency components of the JPS. Since most energy of the signal concentrates on low-frequency components, this elimination reduces the correlation peak. In contrast, besides producing high correlation peak the pre-processing by the AMF with high threshold causes the correlation plane to be noisy. This is because this AMF attenuates less low-frequency components of the JPS than that with low threshold.

Figures 3.3(c) and 3.3(d) show the 3-D plots of the correlation outputs of the noisy high-contrast fingerprint with noise variance $\sigma^2 = 1$ pre-processed by using the AMF with $N = 64.7\%$ and $N = 99.8\%$, respectively. It is obvious that the desired correlation peaks are still sharp with the FAHMs of 1×1 pixel. In comparison with Figs. 3.3(a) and 3.3(b), the presence of noise in the input plane causes simultaneously the decrease in the peak intensities by about one order of magnitude and the increase in noise in the correlation plane. Since the spectrum of the noise extends over the entire frequency domain, however, the use of the AMF with low threshold cannot reduce totally the noise. As a result, the noise in the correlation plane and the peak intensity of Fig. 3.3(d) are higher than those of Fig. 3.3(c).

The correlation outputs of the modified AMJTC of the noise-free low-contrast fingerprint target pre-processed by the AMF with $N = 64.7\%$ and $N = 99.8\%$ are plotted in Figs. 3.4(a) and 3.4(b), respectively. In comparison with Figs. 3.3(a) and 3.3(b), similar correlation outputs with lower peaks are obtained, because the contrast ratio c_T which is smaller than 1 reduces the output of the first correlation term of Eq. (3.5). The correlation outputs of the noise-corrupted low-contrast fingerprint targets pre-processed with $N = 64.7\%$ and $N = 99.8\%$ are shown in Figs. 3.4(c) and 3.4(d), respectively. The further decrease in the correlation peaks and the increase in noise in the correlation plane are caused by the noise which is stronger than the luminance of the low-contrast fingerprint target (Widjaja and Suripon, 2004; Widjaja and Suripon, 2005). As a consequence, the first correlation term of Eq. (3.5) is smaller than the second term. Thus with the same noise level, Figs. 3.3(c) and 3.3(d) contain higher correlation peaks.
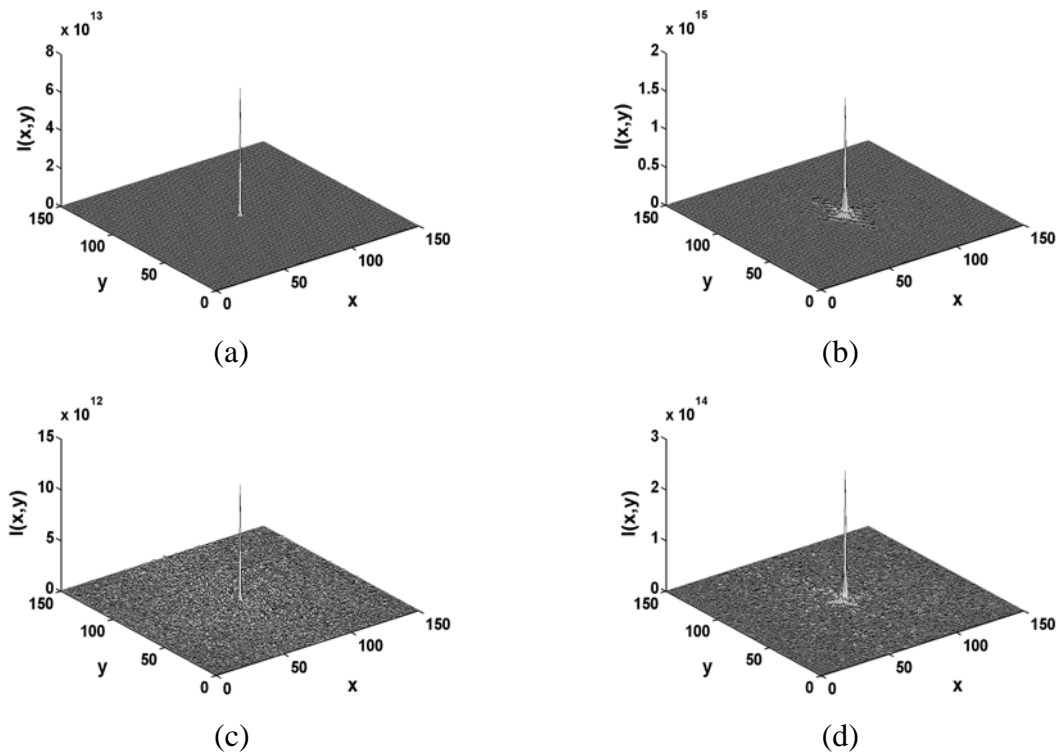
Figure 3.3 Autocorrelation outputs of noise-free high-contrast fingerprint pre-processed by the AMF with (a) $N = 64.7\%$ and (b) $N = 99.8\%$. Cross-correlation outputs of noise-free high-contrast fingerprint reference and noisy high-contrast fingerprint target pre-processed by the AMF with (c) $N = 64.7\%$ and (d) $N = 99.8\%$.

Figure 3.4 Cross-correlation outputs of noise-free high-contrast fingerprint reference and noise-free low-contrast fingerprint target pre-processed by the AMF with (a) $N = 64.7\%$ and (b) $N = 99.8\%$. Cross-correlation outputs of noise-free high-contrast fingerprint reference and noisy low-contrast fingerprint target pre-processed by the AMF with (c) $N = 64.7\%$ and (d) $N = 99.8\%$.

Figure 3.5 shows the variation of the normalized PCDs as a function of the percentage N for different targets detected by using high-contrast fingerprint reference. The normalized PCDs of the noise-free high- and low-contrast fingerprint targets coincide, because scaling of the first correlation term of Eq. (3.5) by the contrast ratio affects both the correlation peak and the standard deviation of the correlation intensity. It is obvious that when the percentage N reduces, the normalized PCDs increase gradually. This occurs because at high percentage N the AMF

attenuates less low-spatial-frequency components than that at low percentage. As a consequence the standard deviation of the correlation intensities at high percentage N is much higher than that at low N. Therefore, the normalized PCD at small percentage N is higher than that at high percentage.
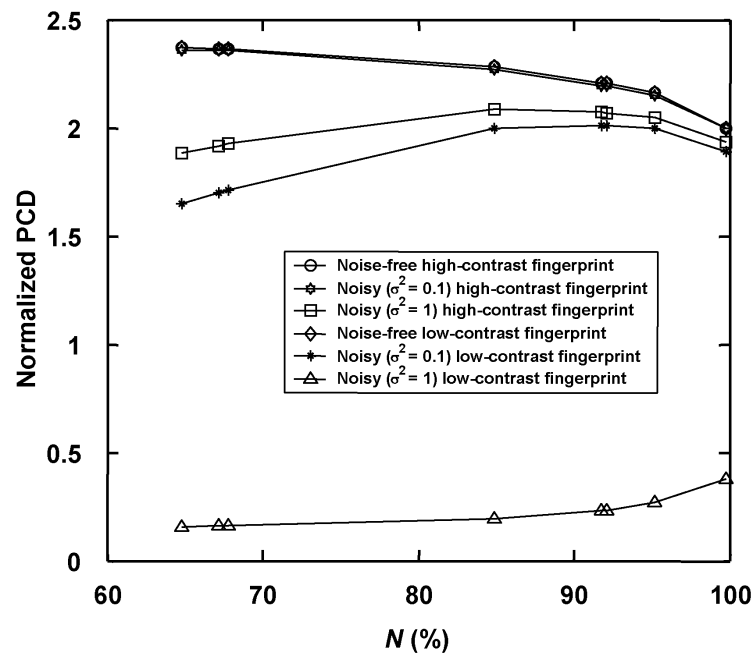
Figure 3.5   The normalized PCD as a function of the percentage N of high-contrast fingerprint reference.

As can be seen in Figs. 3.3 and 3.4, when the input targets are corrupted by strong noise such as with variance $\sigma^2 = 1$, the desired correlation peak decreases and the noise in the correlation plane increases. It is found that the standard deviation of the correlation intensities is always lower than the correlation peak regardless of the threshold values. As the percentage N reduces the standard deviation decreases at a slower rate compared to the decrease of the correlation peak. This is because the noise cannot be totally eliminated by the AMF with low percentage N. For this reason, the

normalized PCD of the detection of the noisy high-contrast fingerprint at low percentage N is lower than that at high percentage.

Unlike the noisy high-contrast fingerprint, in the detection of the noisy low-contrast target the modified AMJTC is not robust to noise. As the variance of the noise increases to 1 the normalized PCD reduces sharply, to less than 0.4. As shown in Figs. 3.4(c) and 3.4(d), this is mainly caused by the decrease in the first correlation term of Eq. (3.5) and the presence of noise. As the threshold value becomes higher, the desired correlation peak increases. Consequently, the normalized PCD at high percentage N is slightly higher than that at low percentage. Therefore, the detection of the low-contrast fingerprint target by the modified AMJTC depends on the noise level in the input plane. In the case of the presence of strong noise, the detection of the low-contrast target may not be accomplished. In order to obtain high normalized PCDs, the detection of the noise-free target should be done by using the AMF with low threshold while, for the detection of the noisy high-contrast fingerprint target, the threshold value should be high.

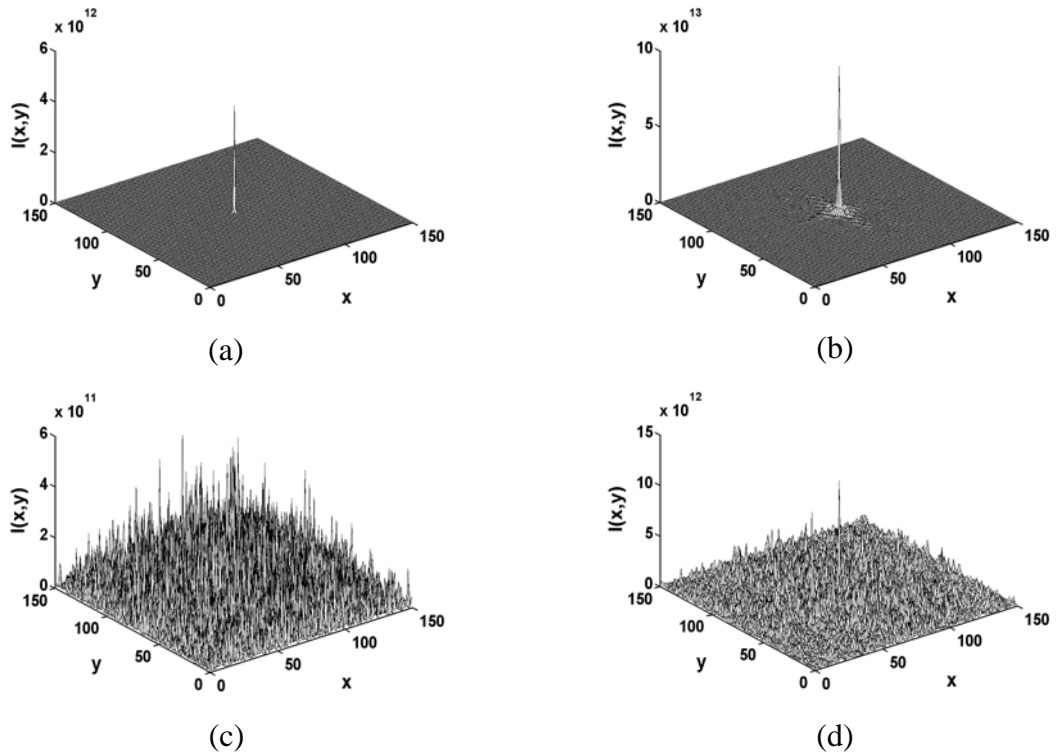### 3.3.2 Low-contrast fingerprint as the reference image

Figures 3.6(a) and 3.6(b) show the 3-D autocorrelation outputs of the noise-free low-contrast fingerprint targets pre-processed by using the AMF with $N = 64.7\%$ that corresponds to low threshold and $N = 99.8\%$ that corresponds to high threshold, respectively. In comparison with Figs. 3.3(a) and 3.3(b), the results are similar in that the autocorrelation width of the low-contrast fingerprint detection is as sharp as that of the high-contrast fingerprint. Their FAHMs always equal to 1×1 pixel. Due to the low contrast of the image, however the correlation peak intensities are reduced by about two orders of magnitude. At high threshold value of the AMF, the correlation plane

also appears to be noisy. The correlation outputs of the noisy target with variance $\sigma^2 =$ 1 are shown in Figs. 3.6(c) and 3.6(d). It is obvious that the correlation peaks become lower and the correlation planes of Figs. 3.6(c) and 3.6(d) become less noisy compared to Figs. 3.4(c) and 3.4(d). This occurs because the correlation of the low-contrast reference and the noise produces smaller output intensity than that of high-contrast image.

The 3-D correlation outputs of the detection of the noise-free high-contrast fingerprint target pre-processed by the AMF with $N = 64.7\%$ and $N = 99.8\%$ are shown in Figs. 3.7(a) and 3.7(b), respectively. Since the contrast ratio is greater than unity, the first correlation term of Eq. (3.5) produces higher correlation peaks than the autocorrelation outputs of the noise-free low-contrast target shown in Fig. 3.6. Following the preceding discussion, the differences of the peak intensities and the noise in the correlation plane between Figs. 3.7(a) and 3.7(b) are caused by the effect of the threshold. Figures 3.7(c) and 3.7(d) show the correlation outputs of the noisy high-contrast target. Since the luminance value of the target image is higher than the noise, the desired correlation peak that is one order of magnitude lower than that of the noise-free case is still distinguishable. In this detection, the FAHM of the correlation signal does not change.
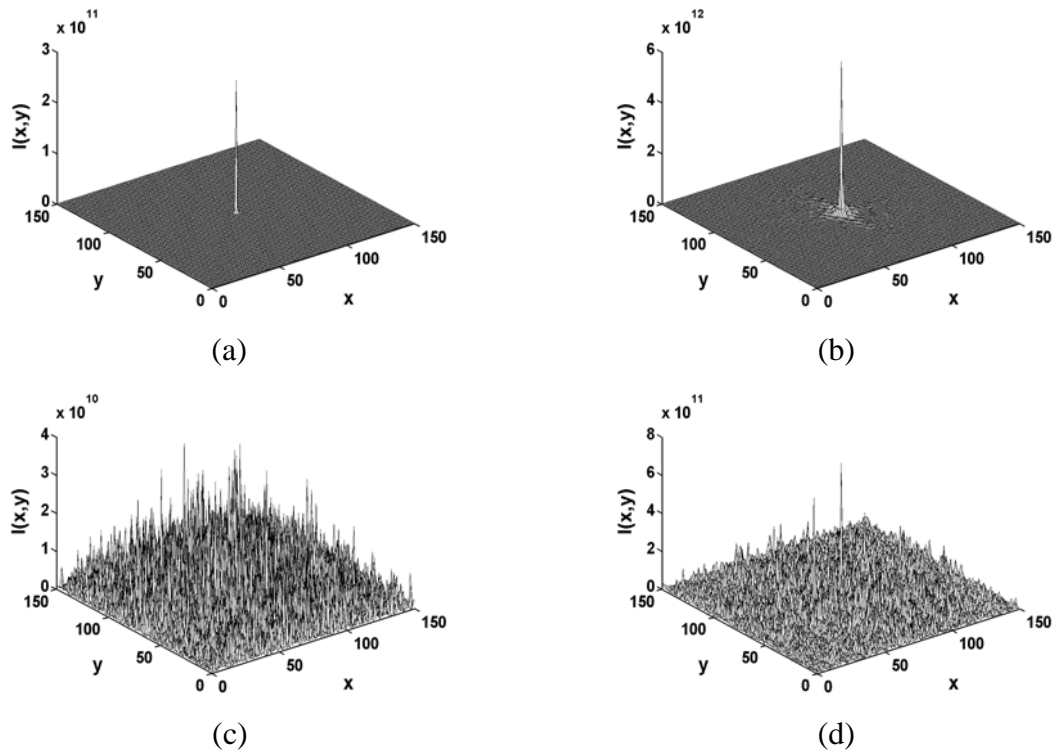
Figure 3.6 Autocorrelation outputs of noise-free low-contrast fingerprint pre-processed by the AMF with (a) $N = 64.7\%$ and (b) $N = 99.8\%$. Cross-correlation outputs of noise-free low-contrast fingerprint reference and noisy low-contrast fingerprint target pre-processed by the AMF with (c) $N = 64.7\%$ and (d) $N = 99.8\%$.
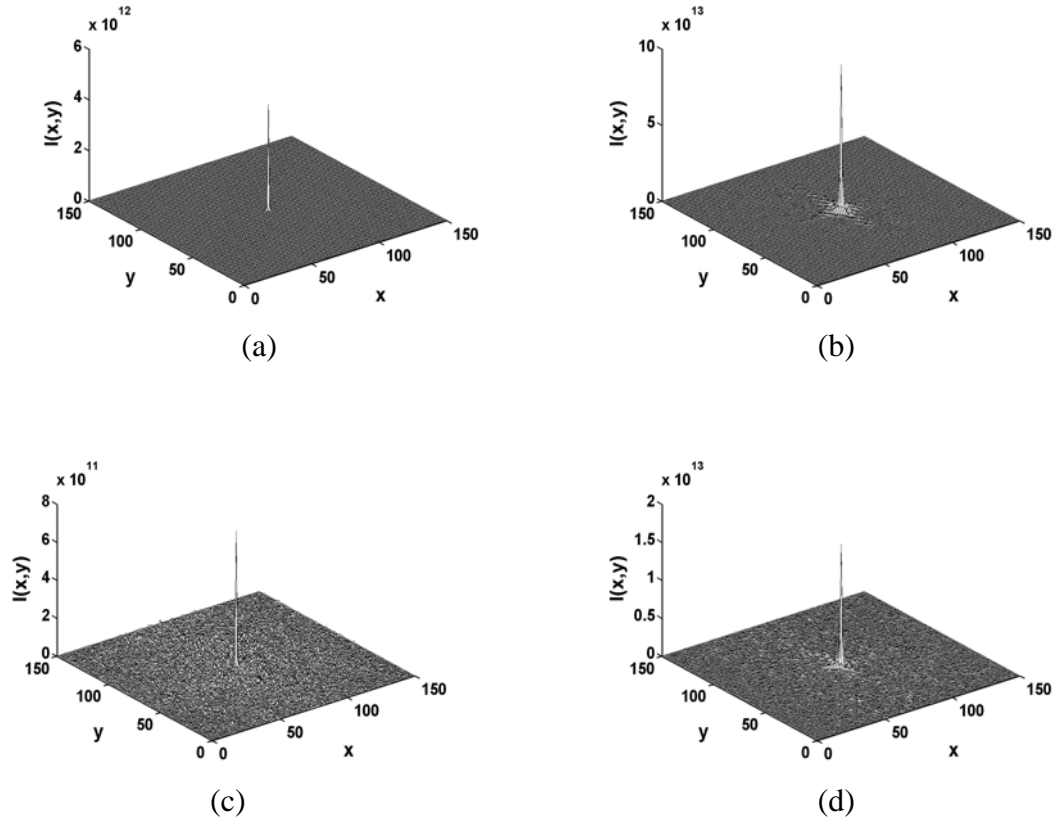
Figure 3.7 Cross-correlation outputs of noise-free low-contrast fingerprint reference and noise-free high-contrast fingerprint target pre-processed by the AMF with (a) $N = 64.7\%$ and (b) $N = 99.8\%$. Cross-correlation outputs of noise-free low-contrast fingerprint reference and noisy high-contrast fingerprint target pre-processed by the AMF with (c) $N = 64.7\%$ and (d) $N = 99.8\%$.

From the computation of the normalized PCDs for different targets detected by using the low-contrast fingerprint reference as a function of the percentage N that is illustrated in Fig. 3.8, it is found that the resultant normalized PCDs are the same as the simulation results produced by using the high-contrast fingerprint reference. This occurs because of the same reason as discussed in the previous section. Besides

having the same conclusion as the ones drawn in the preceding section, this result

reveals that the performance of the modified AMJTC by using high-spatial-frequency

reference images does not depend on the contrast of the reference, but is determined

by the contrast of the target image and the noise present in the input plane.
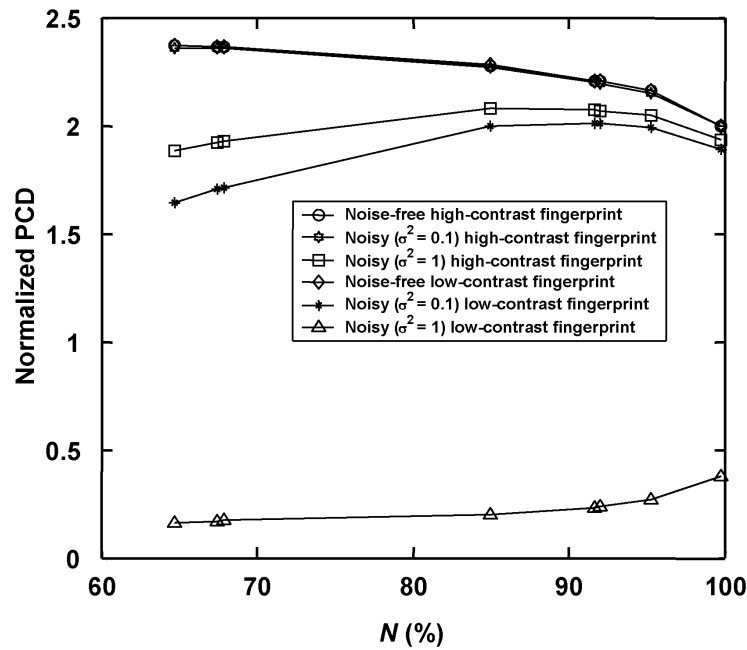
Figure 3.8   The normalized PCD as a function of the percentage N of low-contrast

fingerprint reference.

3.3.3 High-contrast human face as the reference image

The autocorrelation outputs of the noise-free high-contrast human faces pre-

processed by the AMF with $N = 96.3\%$ that corresponds to low threshold and $N =$

99.9% that corresponds to high threshold are illustrated in Figs. 3.9(a) and 3.9(b),

respectively. In comparison with the results of the fingerprint detection, the

autocorrelation peak of the human face image is broader because the human face

image contains less high-spatial-frequency components. By using the human face as

the reference, the impulse response of the JTC becomes broader than that of the

fingerprint reference (Widjaja and Suripon, 2005). As shown in Fig. 3.9(a), the use of the AMF with low threshold gives sharper and lower correlation peak than that of Fig. 3.9(b). This is the result of the edge enhancement of the AMF in which low-spatial-frequency components of the modified JPS are attenuated. Figures 3.9(c) and 3.9(d) are the correlation outputs of the detection of the noisy high-contrast human face targets with variance $\sigma^2 = 1$ by using the AMF $N = 96.3\%$ and $N = 99.9\%$, respectively. Although the preceding results show that the pre-processing of the JPS of the noisy target by using the AMF filter with high threshold gives noisy correlation output, the correlation planes of Figs. 3.9(b) and 3.9(d) do not appear to be noisy. This occurs because the noise components are smoothed out by the broad impulse response. However in the case of pre-processing by the AMF with low threshold, the edge enhancement effect sharpens the noise components.

Figures 3.10(a) and 3.10(b) present the correlation outputs of the low-contrast human face detections obtained by using the AMF with $N = 96.3\%$ and $N = 99.9\%$, respectively. The widths of the correlation signals become as broad as Figs. 3.9(a) and 3.9(b), while, their peak intensities are lower. This is because the target has a lower contrast compared to the reference. The desired correlation is scaled by the contrast ratio that is smaller than unity. Since the luminance of the low-contrast human face is smaller than the noise with variance $\sigma^2 = 1$, the detection of the corrupted low-contrast target produces noisy correlation plane as shown in Figs. 3.10(c) and 3.10(d).
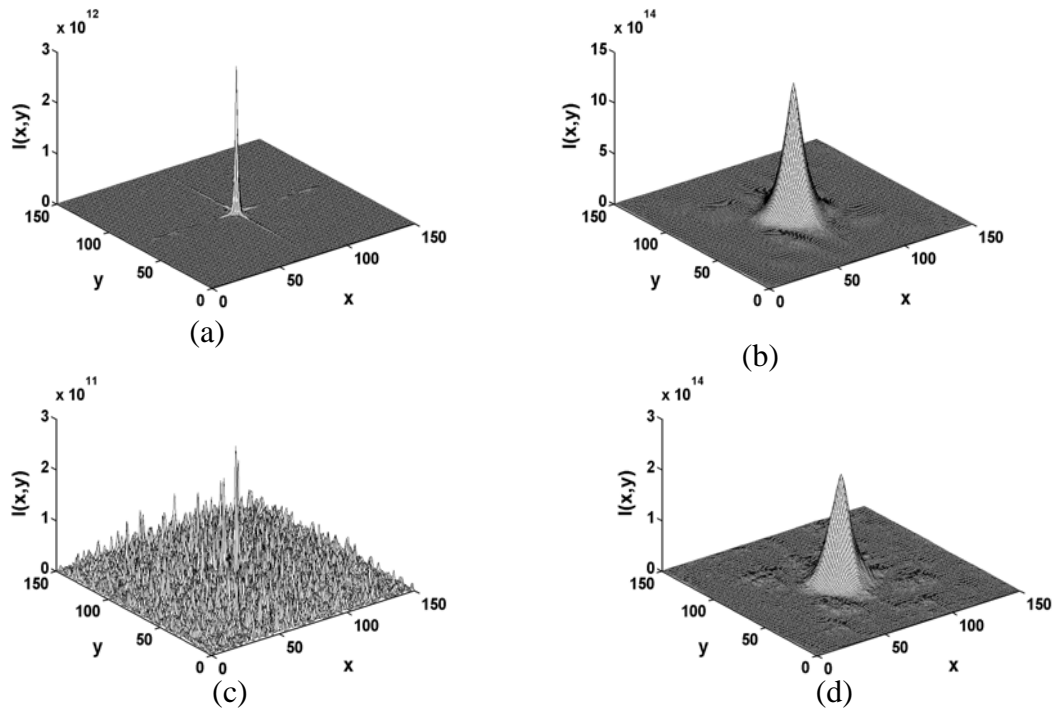
Figure 3.9 Autocorrelation outputs of noise-free high-contrast human face pre-processed by the AMF with (a) $N = 96.3\%$ and (b) $N = 99.9\%$. Cross-correlation outputs of noise-free high-contrast human face reference and noisy high-contrast human face target pre-processed by the AMF with (c) $N = 96.3\%$ and (d) $N = 99.9\%$.
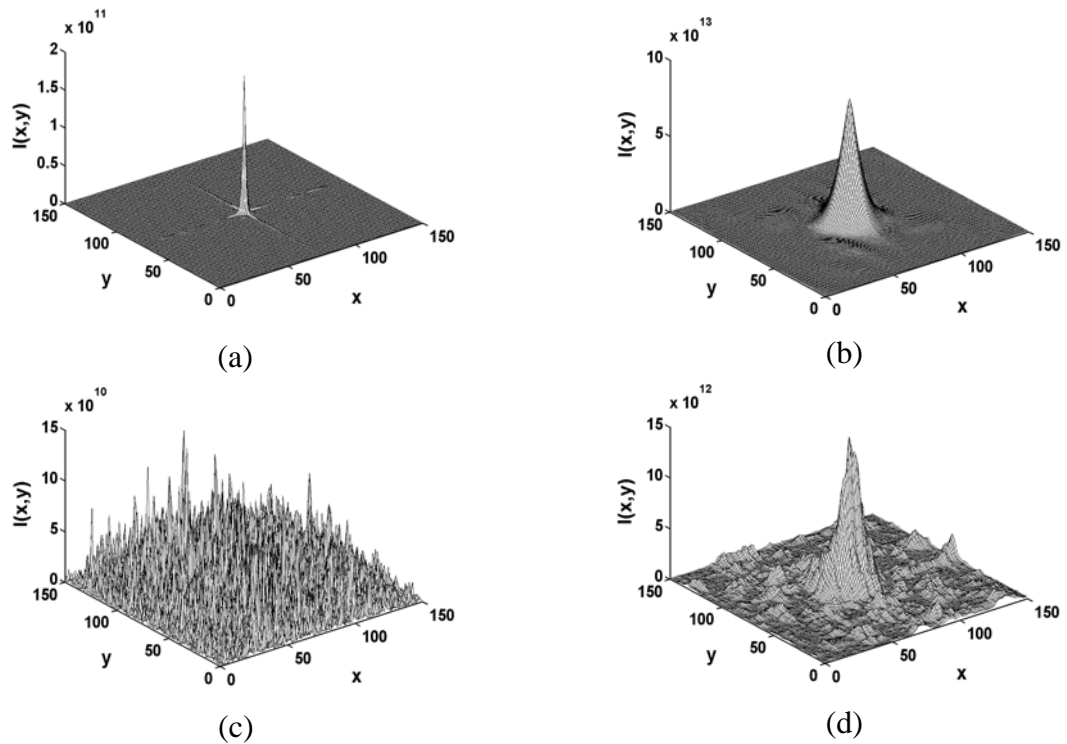
Figure 3.10 Cross-correlation outputs of noise-free high-contrast human face reference and noise-free low-contrast human face target pre-processed by the AMF with (a) $N = 96.3\%$ and (b) $N = 99.9\%$. Cross-correlation outputs of noise-free high-contrast human face reference and noisy low-contrast human face target pre-processed by the AMF with (c) $N = 96.3\%$ and (d) $N = 99.9\%$.
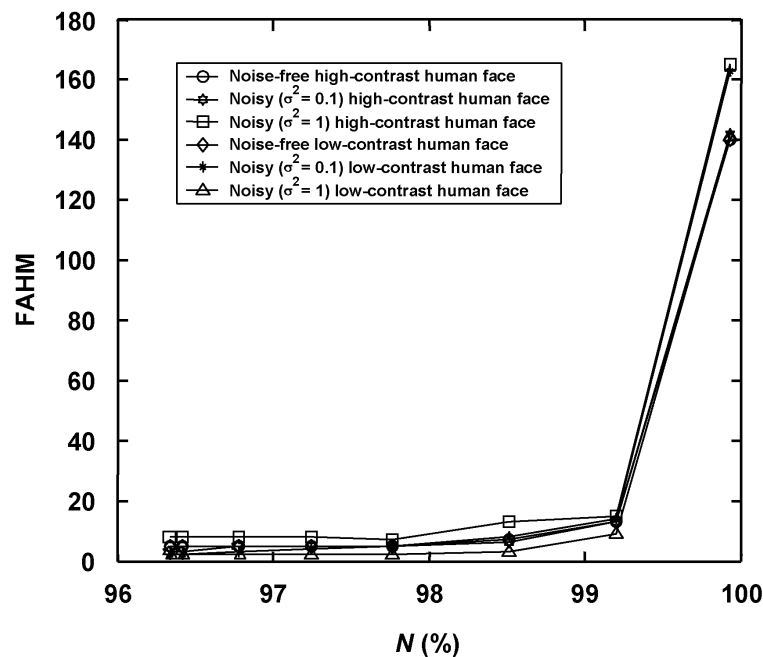
Figure 3.11   The FAHM as a function of the percentage N of high-contrast human

face reference.

Figure 3.11 shows the FAHMs of the modified AMJTC by using high-contrast

human face reference as a function of the threshold percentage N for different targets.

It is clear that the FAHMs depend on the percentage N. When the percentage number

of pixels of the AMF with unity amplitude is 99.9%, the FAHMs of the noisy high-

and low-contrast human faces are the broadest because they contain the summation of

two broad correlation outputs. At the same percentage N, the FAHMs of the detection

of different targets are smaller with almost the same values. When the percentage N

becomes 99.2%, all the FAHMs fall sharply. This is mainly caused by the fact that the

modified JPS contains narrow band of frequency components whose power decreases

rapidly as the frequency becomes higher. Although the percentage N reduces slightly,

most low-spatial-frequency components of the JPS is significantly attenuated. This

sharpens the correlation peaks. As the percentage N reduces further, the FAHMs reduce slowly, because the variation of the power spectrum at higher spatial-frequencies is insignificant. The attenuation of these spatial-frequency components does not sharpen effectively the correlation peaks.
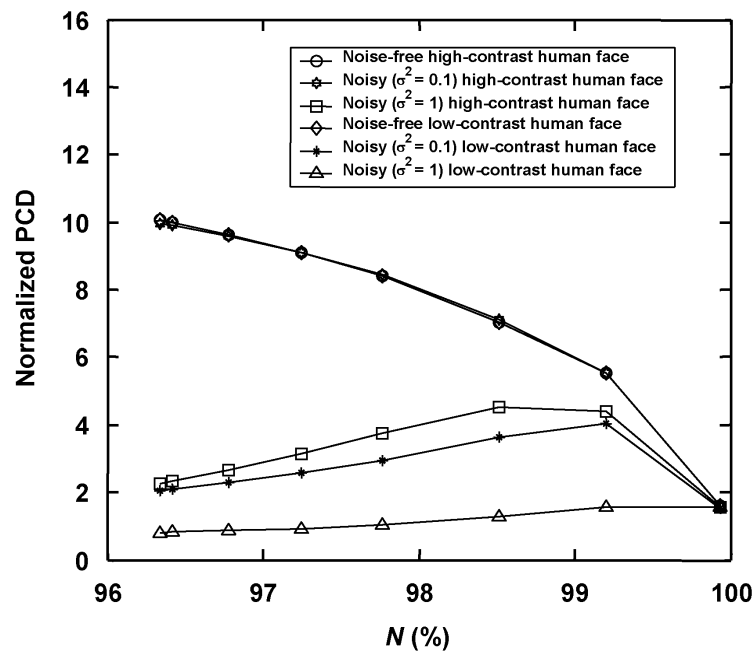
Figure 3.12 The normalized PCD as a function of the percentage N of high-contrast human face reference.

Figure 3.12 shows the normalized PCDs as a function of the percentage N for different target scenes. For the same reason as discussed in the preceding sections, the normalized PCDs of the noise-free high- and low- contrast human face targets are the same. The normalized PCDs at $N = 99.9\%$ is 1.5, because the standard deviation of broad correlation width is much higher than that of the sharp ones. The normalized PCDs increase to be 10 as the percentage N reduces to 96.3%. Although their FAHMs are one order of magnitude greater than that of the noise-free fingerprint detection, the highest value of the normalized PCDs is higher than that of the fingerprint detection.

This is because the value of the PCD of the human face detected by the classical JTC is smaller than that of the fingerprint. When the high-contrast human face target is corrupted by the noise, its normalized PCD at highest percentage N is approximately equal to that of the noise-free detection results because the width of its correlation output is nearly the same. The raise of the normalized PCD to the highest value of 4.5 at $N = 98.5\%$ is followed by a gradual decrease as the percentage N becomes smaller. The high normalized PCD is obtained because the correlation output is sharpened such that the decrease in the standard deviation of the correlation intensity in the correlation plane is greater than that in the peak intensity. Since further decrease in the percentage N attenuates more spatial-frequency components of the JPS, the normalized PCD becomes lower. In the case of the detection of the noisy low-contrast human face target, the degradation of the performance of the modified AMJTC is more severe than the noisy high-contrast target. When the low-contrast human face target is corrupted by noise with variance $\sigma^2 = 1$, its normalized PCD is never higher than 1.6 regardless of the percentage N. Since it is caused by the presence of noise at the input, this detection performance is dependent upon the noise level.

In order to optimize the detection results, the suitable threshold of the AMF must be properly selected from appropriate values of the normalized PCD and the FAHM. For the noise-free targets, the AMF with low threshold should be used for detection because the resultant FAHM is the smallest and the normalized PCD is the highest. However unlike the fingerprint targets, the detection of the noisy high-contrast human face cannot be done by using the AMF with high threshold. The appropriate threshold should be chosen from the sharp FAHM and the highest normalized PCD.

3.3.4 Low-contrast human face as the reference image

Figures 3.13(a) and 3.13(b) show the 3-D autocorrelation of the noise-free low-contrast human face target pre-processed by the AMF with $N = 96.3\%$ that corresponds to low threshold and $N = 99.9\%$ that corresponds to high threshold, respectively. Since the image contrast is low, the correlation peak intensities are lower by about three orders of magnitude than Figs. 3.9(a) and 3.9(b). However, their widths are the same. The effect of using the AMF with low threshold which sharpens and reduces peak of the correlation intensity can be clearly seen from Fig. 3.13(a). In the presence of strong noise with variance $\sigma^2 = 1$, the correlation outputs are degraded as shown in Figs. 3.13(c) and 3.13(d). This is because the luminance of the low-contrast human face image is lower than the noise. According to Eq. (3.5), the second correlation term is greater than the first term. Therefore the desired correlation peak illustrated in Fig. 3.13(c) is indistinguishable.

Figures 3.14(a) and 3.14(b) show the 3-D correlation outputs of the noise-free high-contrast human face target pre-processed. Since the contrast of the target image is higher than that of the reference, the correlation peak intensities are higher than Figs. 3.13(a) and 3.13(b). For this reason, the correlation peak can be observed from Fig. 3.14(c) although the input target is corrupted by strong noise.
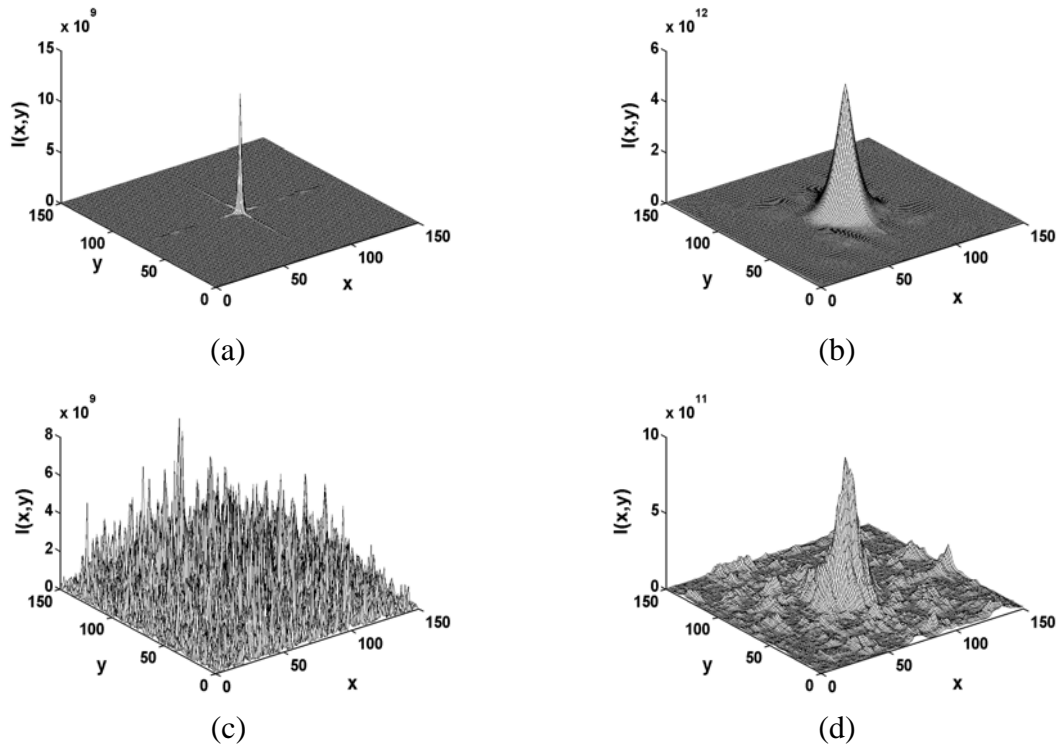
Figure 3.13 Autocorrelation outputs of noise-free low-contrast human face pre-processed by the AMF with (a) $N = 96.3\%$ and (b) $N = 99.9\%$. Cross-correlation outputs of noise-free low-contrast human face reference and noisy high-contrast human face target pre-processed by the AMF with (c) $N = 96.3\%$ and (d) $N = 99.9\%$.

(a)

(b)

(c)

(d)
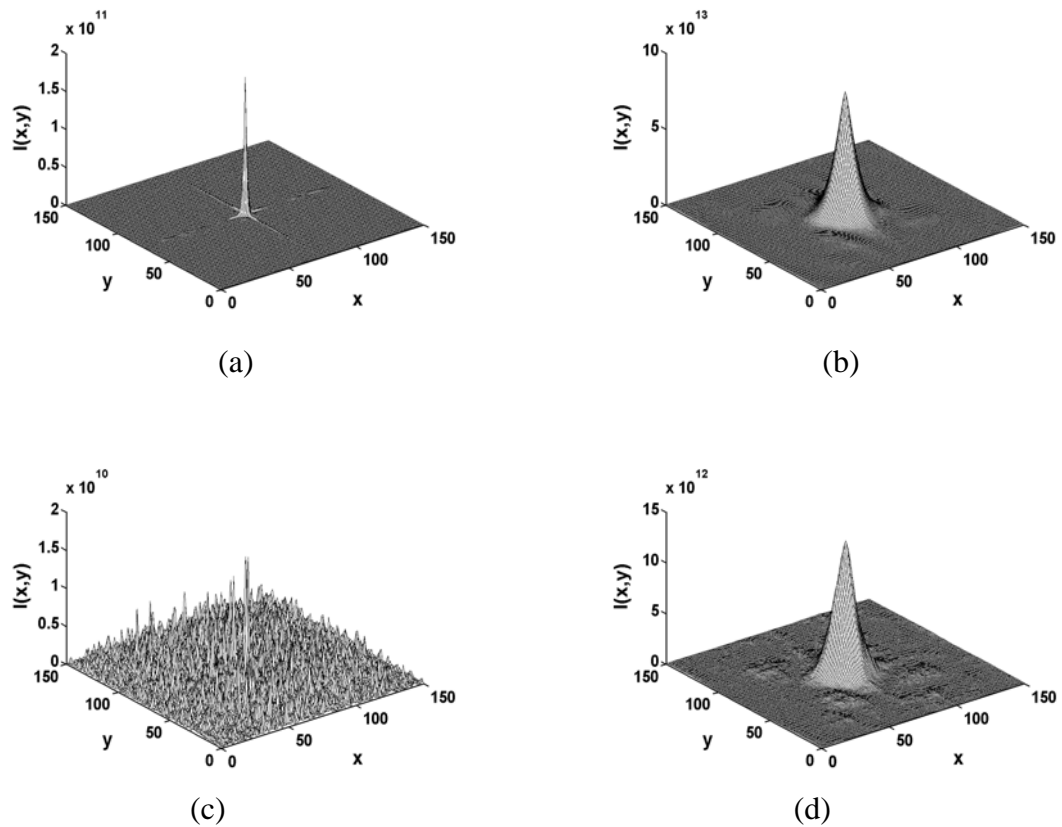
Figure 3.14   Cross-correlation outputs of noise-free low-contrast human face reference and noise-free high-contrast human face target pre-processed by the AMF with (a) N = 96.3% and (b) N = 99.9%. Cross-correlation outputs of noise-free low-contrast human face reference and noisy high-contrast human face target pre-processed by the AMF with (c) N = 96.3% and (d) N = 99.9%.

Figures 3.15 and 3.16 show the FAHMs and the normalized PCDs of the modified AMJTC by using low-contrast human face reference. The results are almost the same as the result of the high-contrast reference. This is because of the same reason as discussed in the previous section.
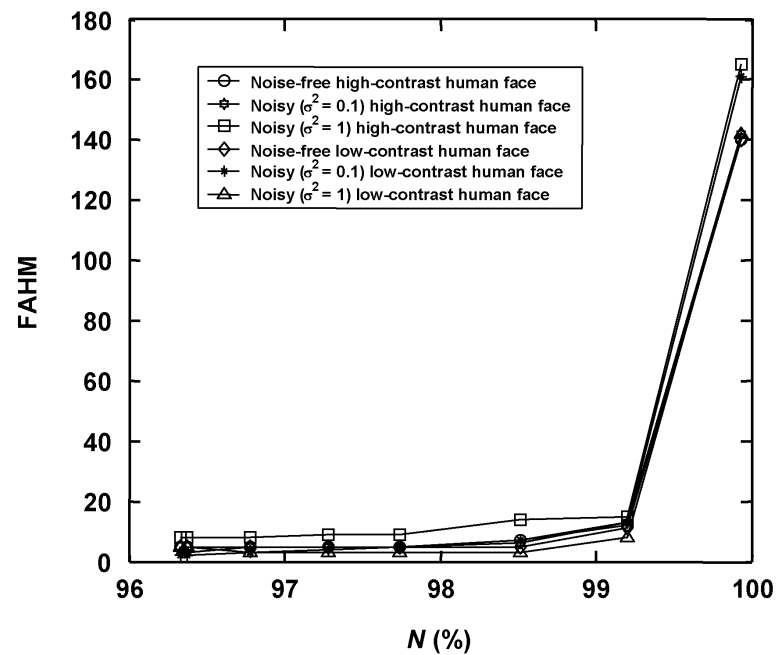
Figure 3.15 The FAHM as a function of the percentage N of low-contrast human face
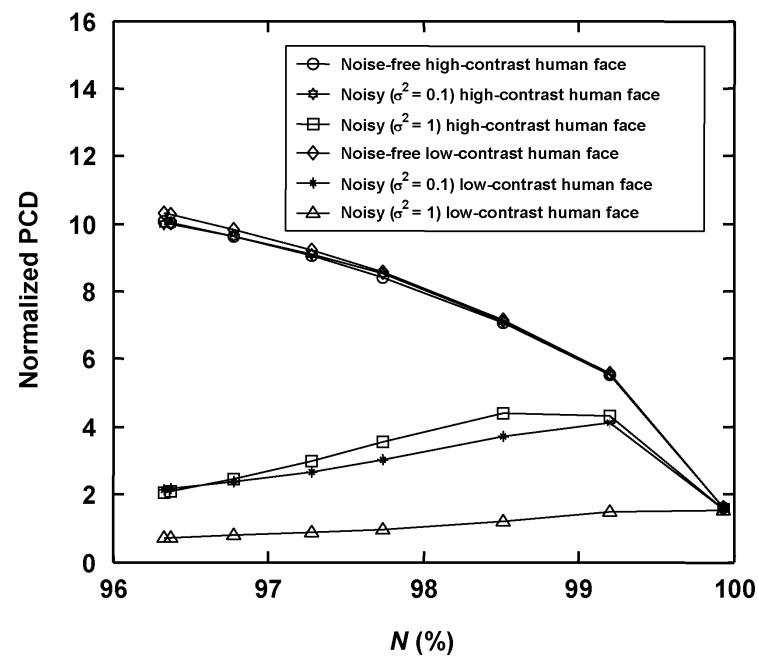
reference.

Figure 3.16 The normalized PCD as a function of the percentage N of low-contrast

human face reference.

Table 3.1 summarizes the optimization condition for the modified AMJTC. It can be concluded from this table that the detection performance can be optimized by selecting appropriate threshold value, which depends on the noise level in the input, the contrast and the spatial-frequency content of the target.

Table 3.1 Optimization condition for single-target detection by using the modified AMJTC

Reference images	Condition for target images			
	Noise free		Noisy	
	High contrast	Low contrast	High contrast	Low contrast
High-contrast fingerprint	Low threshold	Low threshold	High threshold	None
Low-contrast fingerprint	Low threshold	Low threshold	High threshold	None
High-contrast human face	Low threshold	Low threshold	Intermediate threshold	Intermediate threshold
Low-contrast human face	Low threshold	Low threshold	Intermediate threshold	Intermediate threshold

CHAPTER IV

EFFECTS OF THRESHOLD ON MULTIPLE-TARGET

DETECTION

In the previous chapter, the effect of threshold on the single-target detection using the modified AMJTC was studied. The simulation results show that the performance of the single-target detection can be optimized by selecting appropriate threshold value. Its performance depends on the noise level in the input, the contrast and the spatial-frequency content of the target. Furthermore, the human face detection can be improved greater than that of fingerprint. In the case of low-contrast target with high-spatial frequency content, the modified AMJTC is not tolerant to noise.

In real-world applications, the input scenes may consist of a desired target cluttered with unwanted objects. Thus, a study of discrimination ability of the modified AMJTC is important. In this chapter the effect of threshold on multiple-target detection using modified AMJTC is further studied by using computer simulation with the same type of images. To measure the discrimination ability of the modified AMJTC, the PSR is used.

4.1 Detection of noisy multiple target with different contrast

Consider an input scene $t_i(x, y)$ consisting of M wanted and unwanted target images is captured by the CCD2 and stored into the computer of the optical setup shown in Fig. 2.1. The generated power spectrum of the input scene is also stored into the computer in the same way as that of the reference image. The reference $r(x, y)$

and the input scene $t_i(x, y)$ are then displayed side-by-side with a separation of $2x_0$ on the EASLM. This joint input image can be mathematically expressed as

$$f(x, y) = r(x - x_0, y) + \sum_{i=1}^{M} t_i(x + x_i + x_0, y + y_i), \qquad (4.1)$$

where x_i and y_i are the relative position of the target in the x and y directions, respectively. When the input scene is corrupted by the noise and the reference and the target images have the contrast difference, the joint input image can be rewritten as

$$f(x, y) = r(x - x_0, y) + c_T \sum_{i=1}^{M} t_i(x + x_i + x_0, y + y_i) + n(x + x_0, y). \qquad (4.2)$$

The EASLM is then illuminated perpendicularly by a coherent plane wave. By means of the lens L1, the Fourier spectrum of the joint image is obtained at the back focal plane of the lens and is subsequently captured by the CCD1. Its captured JPS can be mathematically expressed as

$$
\begin{aligned}
|F(f_x, f_y)|^2 = {} & |R(f_x, f_y)|^2 + c_T^2 \sum_{i=1}^{M} |T_i(f_x, f_y)|^2 + |N(f_x, f_y)|^2 \\
& + c_T \left\{ N(f_x, f_y) \sum_{i=1}^{M} T_i^*(f_x, f_y) \exp\left[-j2\pi\left(x_i f_x + y_i f_y\right)\right] \right. \\
& \left. + N^*(f_x, f_y) \sum_{i=1}^{M} T_i(f_x, f_y) \exp\left[j2\pi\left(x_i f_x + y_i f_y\right)\right] \right\} \\
& + c_T^2 \left[\sum_{\substack{i=1}}^{M} \sum_{\substack{k=1 \\ k \neq i}}^{M} T_i^*(f_x, f_y) T_k(f_x, f_y) \exp\left\{-j2\pi\left[\left(x_i - x_k\right)f_x + \left(y_i - y_k\right)f_y\right]\right\} \right. \\
& \left. + \sum_{\substack{i=1}}^{M} \sum_{\substack{k=1 \\ k \neq i}}^{M} T_i(f_x, f_y) T_k^*(f_x, f_y) \exp\left\{j2\pi\left[\left(x_i - x_k\right)f_x + \left(y_i - y_k\right)f_y\right]\right\} \right] \\
& + c_T \left[R(f_x, f_y) \sum_{i=1}^{M} T_i^*(f_x, f_y) \exp\left\{-j2\pi\left[\left(x_i + 2x_0\right)f_x + y_i f_y\right]\right\} \right. \\
& \left. + R^*(f_x, f_y) \sum_{i=1}^{M} T_i(f_x, f_y) \exp\left\{j2\pi\left[\left(x_i + 2x_0\right)f_x + y_i f_y\right]\right\} \right]
\end{aligned}
$$

$$+ R(f_x, f_y) N^*(f_x, f_y) \exp(-j4\pi x_0 f_x)$$
$$+ R^*(f_x, f_y) N(f_x, f_y) \exp(j4\pi x_0 f_x), \tag{4.3}$$

where $T_i(f_x, f_y)$ stands for the Fourier transform of the *i*th target and the noise. The first three terms of Eq. (4.3) correspond to the autocorrelations of the reference, the input scene, and the noise, respectively. The cross-correlations between the input scene and the noise are in the fourth and the fifth terms, while the sixth and the seventh terms associate with the cross-correlation between different targets, where the orders of the terms are numbered by ignoring the outer braces and brackets. The eighth and the ninth terms denote the cross-correlation between the reference and all targets and the last two terms represent the cross-correlations between the reference and the noise.

To overcome the problems of a strong zero-order term and the noise terms, the power spectra of the reference and of the noise-corrupted input scene that correspond to the first seven terms of Eq. (4.3) are digitally subtracted from Eq. (4.3) by using a computer (Huang, Lai and Gao, 1997). This subtraction gives

$$U(f_x, f_y) = c_T \left[R(f_x, f_y) \sum_{i=1}^{M} T_i^*(f_x, f_y) \exp \left\{ -j2\pi \left[(x_i + 2x_0) f_x + y_i f_y \right] \right\} \right.$$
$$\left. + R^*(f_x, f_y) \sum_{i=1}^{M} T_i(f_x, f_y) \exp \left\{ j2\pi \left[(x_i + 2x_0) f_x + y_i f_y \right] \right\} \right]$$
$$+ R(f_x, f_y) N^*(f_x, f_y) \exp(-j4\pi x_0 f_x)$$
$$+ R^*(f_x, f_y) N(f_x, f_y) \exp(j4\pi x_0 f_x) \tag{4.4}$$

which shows, in comparison with Eq. (4.3), that not only the dc and some noise terms but also the cross-correlation terms between the targets have been removed. In order to improve the performance of this system and to further reduce the noise, the resultant JPS is modulated by the AMF.

After applying with the AMF, the modified amplitude-modulated JPS can be rewritten as

$$
\begin{aligned}
H_{\text{AMF}}\left(f_x, f_y\right) U\left(f_x, f_y\right) = H_{\text{AMF}}\left(f_x, f_y\right) \times \Bigg\{ & c_T R\left(f_x, f_y\right) \Bigg[\sum_{i=1}^{M} T_i^*(f_x, f_y) \\
& \times \exp\left\{-j2\pi\left[\left(x_i + 2x_0\right)f_x + y_i f_y\right]\right\} \Bigg] \\
& + c_T R^*\left(f_x, f_y\right) \Bigg[\sum_{i=1}^{M} T_i(f_x, f_y) \\
& \times \exp\left\{j2\pi\left[\left(x_i + 2x_0\right)f_x + y_i f_y\right]\right\} \Bigg] \\
& + R\left(f_x, f_y\right) N^*\left(f_x, f_y\right) \exp\left(-j4\pi x_0 f_x\right) \\
& + R^*\left(f_x, f_y\right) N\left(f_x, f_y\right) \exp\left(j4\pi x_0 f_x\right) \Bigg\}.
\end{aligned}
\tag{4.5}
$$

By displaying the modified JPS into the EASLM, the subsequent optical Fourier transform produces the correlation output at the back focal plane of the lens L1 as

$$
\begin{aligned}
c(x, y) &= F^{-1}\left\{H_{\text{AMF}}(f_x, f_y) U(f_x, f_y)\right\} \\
&= c_T h_{\text{AMF}}(x, y) \otimes r(x, y) * \sum_{i=1}^{M} t_i(x, y) \otimes \delta\left[x \pm \left(x_i + 2x_0\right), y \pm y_i\right] \\
&\quad + h_{\text{AMF}}(x, y) \otimes r(x, y) * n(x, y) \otimes \delta\left(x \pm 2x_0, y\right).
\end{aligned}
\tag{4.6}
$$

In Eq. (4.6), the first term scaled by the contrast ratio is the correlation between the reference and the input scene, while the second term is the correlation between the reference and the noise. Although the convolution of $h_{\text{AMF}}(x, y)$ with the first term may optimize the desired detection, the correlation of the wanted target may be corrupted by the correlation of the reference with the unwanted targets and the noise because the input scene consists of multiple targets.

4.2 Computer simulation

In order to study the effects of threshold on multiple-target detection by using

the modified AMJTC, the same test images as in the previous chapter were used. The target and the unwanted target images were combined as the input scene. Figures 4.1(a) and 4.1(b) show the input scene and the reference for high-contrast fingerprint and human face images, respectively, while Figs. 4.1(c) and 4.1(d) for corresponding low-contrast images. In this study, the input scene and the reference image were separated by a distant $2x_0 = 248$ pixels in the area of 832×1116 pixels. The target and the unwanted target images were separated by the distance 186 pixels in the y direction.

(a)

(b)

(c)

(d)
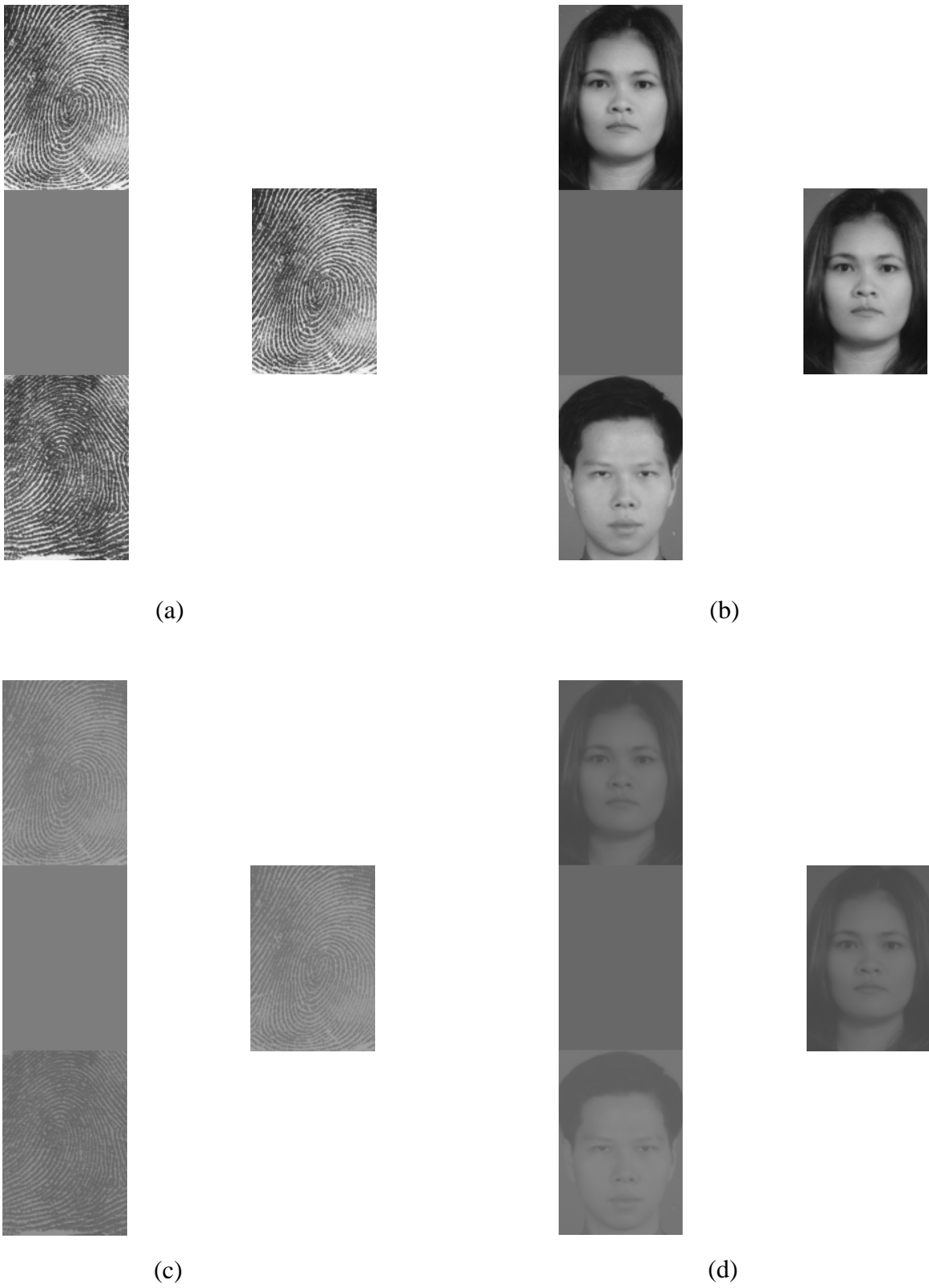
Figure 4.1 Original test images: (a) high-contrast fingerprint, (b) high-contrast human

face, (c) low-contrast fingerprint, and (d) low-contrast human face.

In the case of the multiple-target detection, the correlation output consists of the primary peak due to the cross-correlation between the reference and the target, and the secondary peak due to the cross-correlation between the reference and the unwanted target. Consequently, the detection performance was measured by the PSR of the intensities. A large PSR corresponds to a high discrimination ability of the modified AMJTC, while a small PSR indicates a poor discrimination ability. Even if PSR is sufficiently large, however, the primary peak may be hard to be detected in the presence of strong noise in the correlation plane. Besides the PSR, therefore, the detection performance was also measured by the normalized PCD. They were evaluated as a function of the percentage N. Since the reference images of multiple-target detection are the same as those of the single-target detection, the same threshold values are used.

4.3 Simulation results

4.3.1 High-contrast fingerprint as the reference image

The 3-D correlation outputs of detecting noise-free and high-contrast targets are shown in Figs. 4.2(a) and 4.2(b) for the AMF with (a) $N = 64.7\%$ that corresponds to low threshold and (b) $N = 99.8\%$ that corresponds to high threshold. It is obvious that only the primary peaks can be observed in the both cases, because their intensities are significantly higher than the secondary ones. The full-area at half maximum is equal to 1×1 pixel in either case. In comparison with Fig. 4.2(b), the primary peak of Fig. 4.2(a) is lower by about one order of magnitude and its correlation plane is less noisy since the AMF with the low threshold attenuates the wide range of low-spatial-frequency components of the JPS. Figures 4.2(c) and 4.2(d) present the correlation outputs for the noisy high-contrast targets with variance $\sigma^2 = 1$ pre-processed by the

AMF with the same thresholds as used in Figs. 4.2(a) and 4.2(b), respectively. Although the presence of the strong noise reduces the primary peaks by about one order of magnitude as compared to Figs. 4.2(a) and 4.2(b), their peak intensities are still high.

Figures 4.3(a) and 4.3(b) illustrate the 3-D correlation outputs of detecting noise-free and low-contrast targets pre-processed by the AMF with $N =$ (a) 64.7% and (b) 99.8%. The primary peaks are as sharp as the ones shown in Fig. 4.2, while the secondary peaks are still hard to be observed. Due to the effect of the contrast difference as shown in Eq. (4.6), the primary peaks of Figs. 4.3(a) and 4.3(b) are lower by about one order of magnitude than those of Figs. 4.2(a) and 4.2(b), respectively. The results of the noisy low-contrast targets with variance $\sigma^2 = 1$ are presented in Figs. 4.3(c) and 4.3(d) for the AMF with $N =$ (c) 64.7% and (d) 99.8%. In comparison with Figs. 4.3(a) and 4.3(b), their correlation peak intensities are lower and the correlation plane are noisier. In the case of the low threshold shown in Fig. 4.3 (c), the desired primary peak cannot be distinguished from the noise.

The variation of the PSRs is presented in Fig. 4.4 as a function of the percentage N for different targets detected by using the high-contrast reference. Almost all PSRs are greater than 400 except in the case of the detections of the noisy low-contrast target with variance $\sigma^2 = 1$, where the PSR is about 9. This still ensures that the correlator can discriminate the target from the unwanted target. As the percentage N decreases, the PSRs of the high-contrast targets become higher. This is due to the edge enhancement property of the AMF. Even when the target is of low contrast, the PSR for the noise-free case increases more drastically than those of any other cases as N becomes smaller. This may occur because the spectrum of the

unwanted targets is significantly different from that of the desired target. Consequently, it is easily attenuated by the AMF. Thus, the secondary peak is degenerated faster than the primary peak. In the case of the noisy low-contrast target detections, however, its JPS is severely distorted by the noise. Therefore, as the noise level increases, the PSR becomes lower. Furthermore, as found in the previous chapter, the AMF fails to improve the detection performance. Therefore, in the case of low-contrast target, the performance of the modified AMJTC depends mainly on the noise level.

Figure 4.5 shows the normalized PCDs of the primary peak as a function of the percentage N for different target scenes. Similar results to the previous chapter are found in that the normalized PCD is less than unity only in the case of the noisy low-contrast target with variance $\sigma^2 = 1$. This is because the contrast ratio that is smaller than unity lowers the first correlation term of Eq. (4.6) and the presence of the strong noise in the correlation plane increases the value of its standard deviation. Since the performance of the modified AMJTC must be better than that of the classical JTC, the detection performance of the multiple targets by means of the modified AMJTC can be done by using any threshold value except in the case of the noisy low-contrast target with variance $\sigma^2 = 1$.
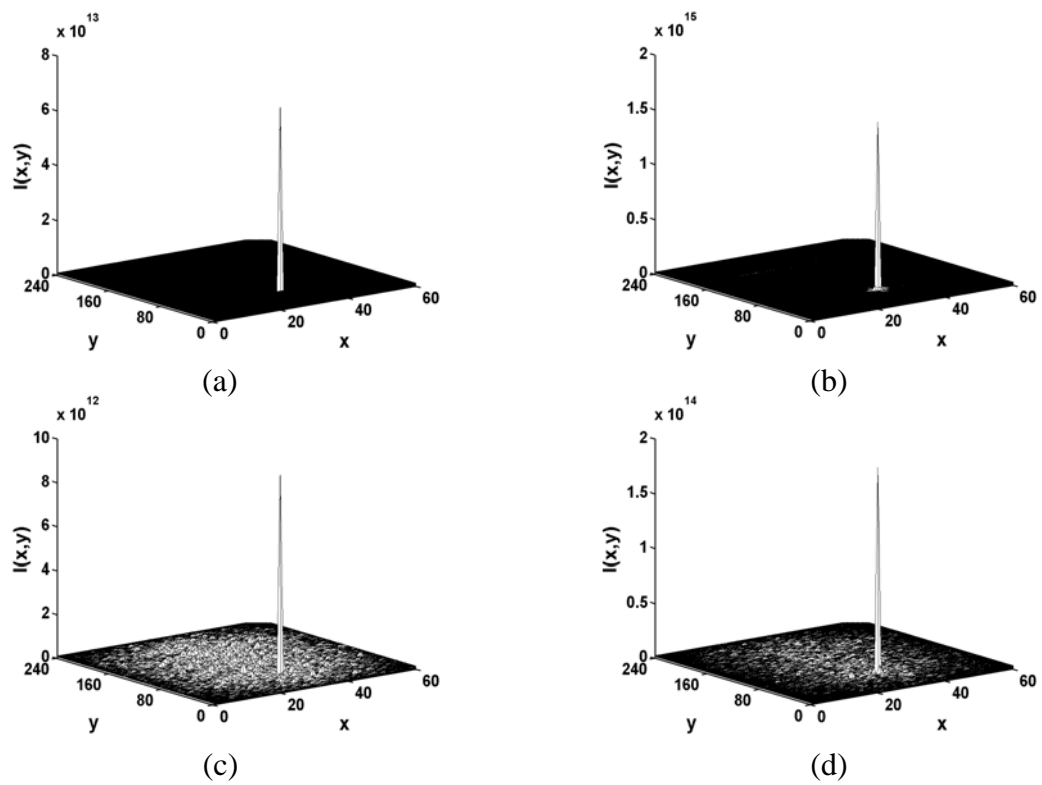
Figure 4.2 Correlation outputs of noise-free high-contrast multiple-fingerprint detections pre-processed by the AMF with $N =$ (a) 64.7% and (b) 99.8%, and of noisy high-contrast target ($\sigma^2 = 1$) pre-processed by the AMF with $N =$ (c) 64.7% and (d) 99.8%
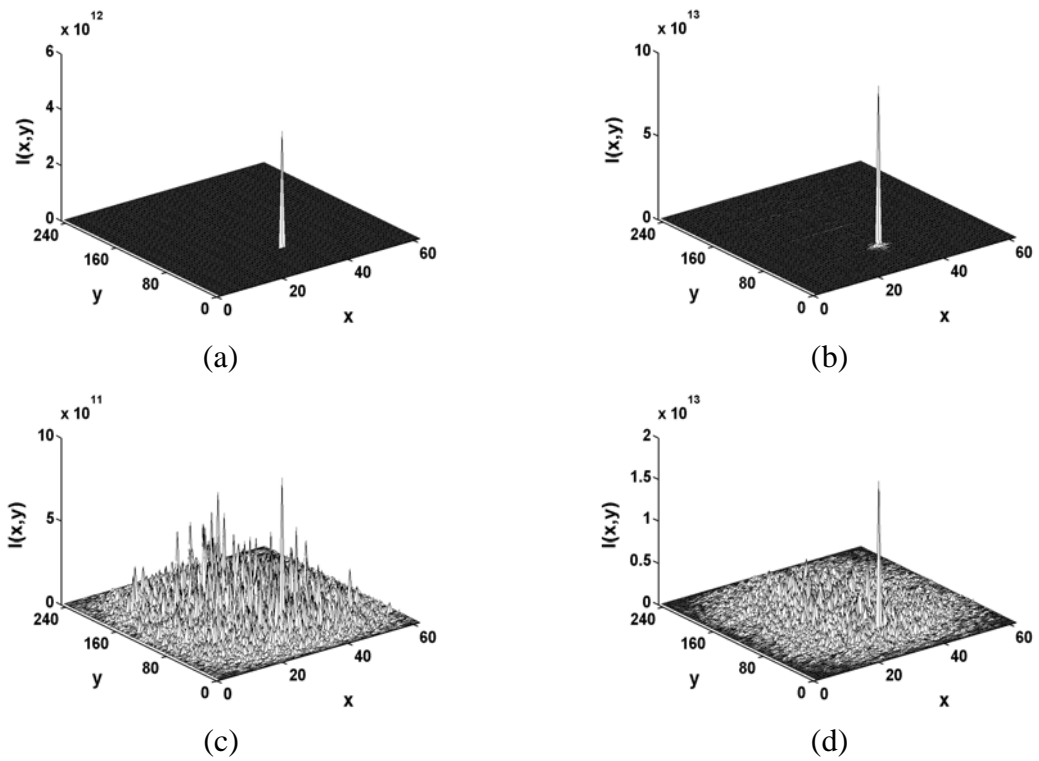
Figure 4.3 Correlation outputs of noise-free low-contrast multiple-fingerprint detections pre-processed by the AMF with $N =$ (a) 64.7% and (b) 99.8%, and of noisy low-contrast target ($\sigma^2 = 1$) pre-processed by the AMF with $N =$ (c) 64.7% and (d) 99.8%.
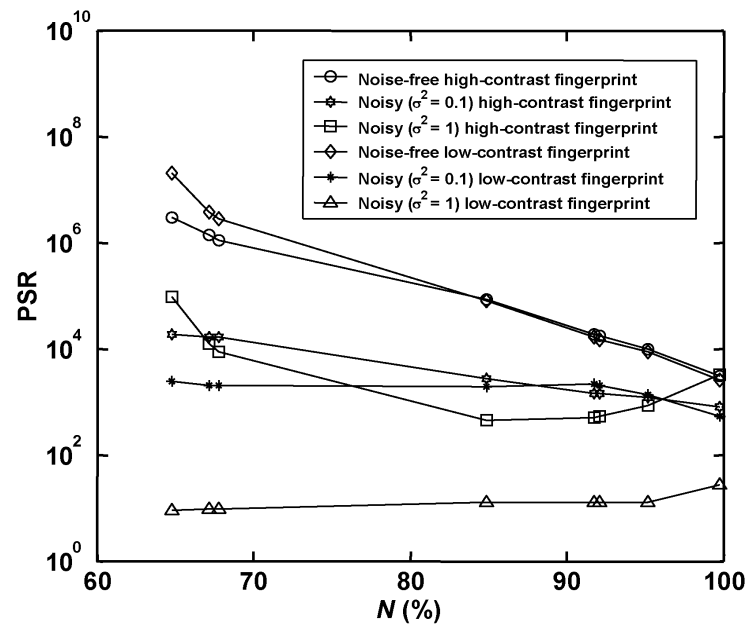
Figure 4.4 PSR as a function of the percentage *N* of high-contrast fingerprint reference.
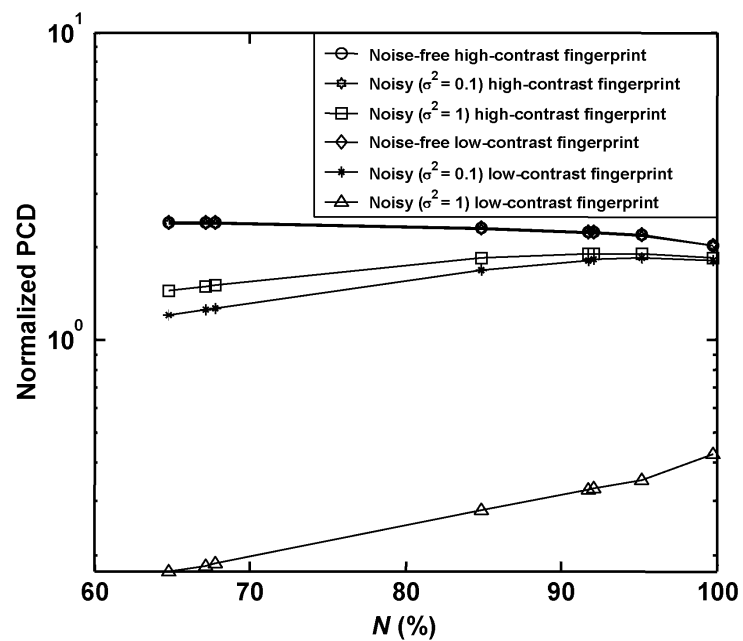
Figure 4.5 Normalized PCD of the primary peak as a function of the percentage *N* of high-contrast fingerprint reference.

4.3.2 Low-contrast fingerprint as the reference image

The 3-D plots of the correlation outputs of detecting noise-free and low-contrast targets are illustrated in Figs. 4.6(a) and 4.6(b) for the AMF with N = (a) 64.7% and (b) 99.8%. The results are similar to Figs. 4.2(a) and 4.2(b), respectively, in that the widths of the primary peaks are the same as those of the high-contrast target detection. However, their peak intensities are lower by about two orders of magnitude, because the image contrast is lower. Figures 4.6(c) and 4.6(d) show the correlation outputs for the noisy low-contrast targets with variance $\sigma^2 = 1$ obtained by the AMF with N = (c) 64.7% and (d) 99.8%. It is obvious that the primary peak of Fig. 4.6(c) is buried in noise because of the presence of the strong noise in the low contrast input scene.

Figures 4.7(a) and 4.7(b) present the cross-correlation outputs for the noise-free high-contrast targets obtained by the AMF with N = (a) 64.7% and (b) 99.8%, while the results for the noisy high-contrast targets with variance $\sigma^2 = 1$ are shown in Figs. 4.7(c) and 4.7(d) for the same AMF as Figs. 4.7(a) and 4.7(b), respectively. The primary peaks of these four cases are higher by about one order of magnitude and the correlation planes are less noisy as compared to Figs. 4.6(a)-(d), respectively. This is because the image contrast is high. Thus, the first correlation term of Eq. (4.6) is larger than the second term. It can be concluded from Figs. 4.2, 4.3, 4.6 and 4.7 that, regardless of the reference contrast, the secondary peak can be suppressed by applying the AMF.

The PSRs and the normalized PCDs of the modified AMJTC by using the low-contrast references give similar results to those of the high-contrast reference because the entire correlation intensities are reduced by the same scale. The PSRs and the

normalized PCDs as a function of the percentage N for different targets detected by using the low-contrast reference are shown in Figs. 4.8 and 4.9, respectively. Thus, the performance of the modified AMJTC for multiple-target detection depends on the contrast of the target and the noise level in the input plane, while not very much on the contrast of the reference. This is in agreement with the result of the single-target detection reported in the previous chapter.

(a)

(b)

(c)

(d)
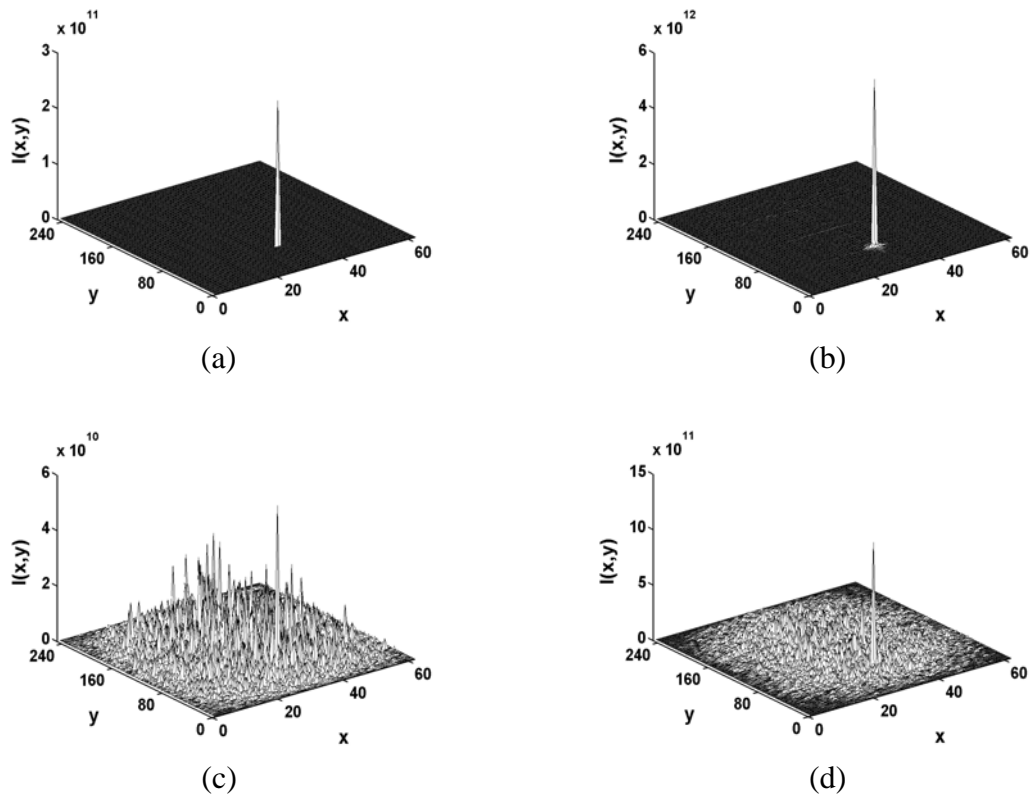
Figure 4.6 Correlation outputs of noise-free low-contrast multiple-fingerprint detections pre-processed by the AMF with $N =$ (a) 64.7% and (b) 99.8%, and of noisy low-contrast target ($\sigma^2 = 1$) pre-processed by the AMF with $N =$ (c) 64.7% and (d) 99.8%
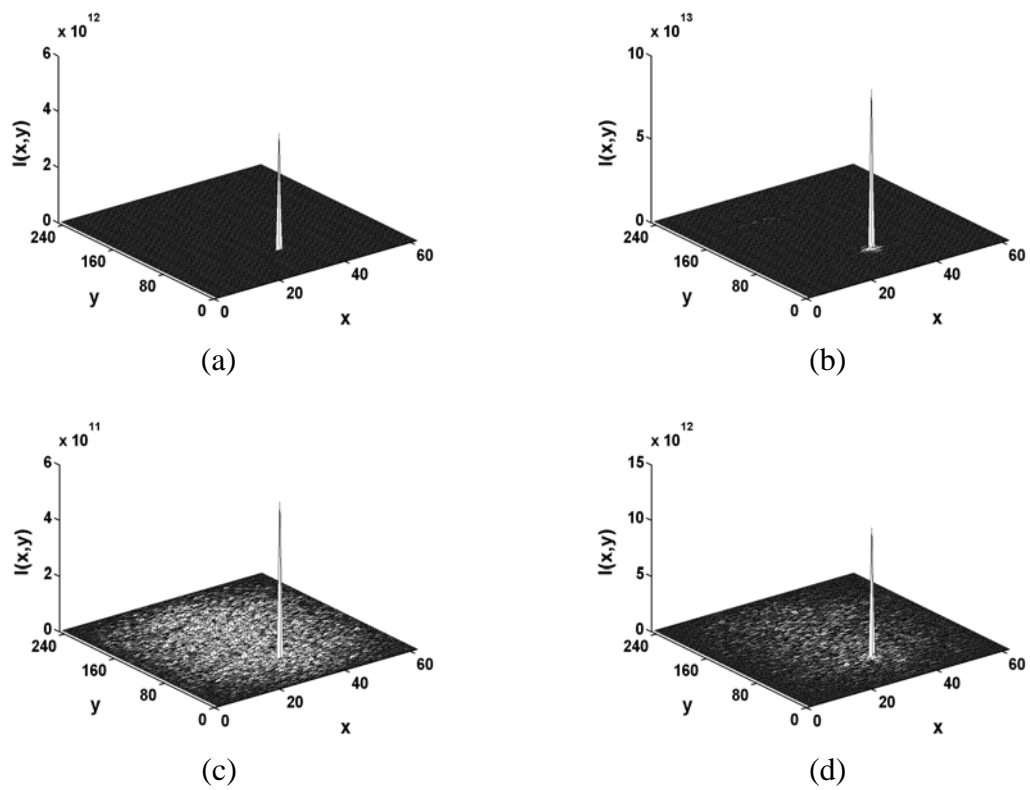
Figure 4.7 Correlation outputs of noise-free high-contrast multiple-fingerprint detections pre-processed by the AMF with N = (a) 64.7% and (b) 99.8%, and of noisy high-contrast target ($\sigma^2 = 1$) pre-processed by the AMF with N = (c) 64.7% and (d) 99.8%.
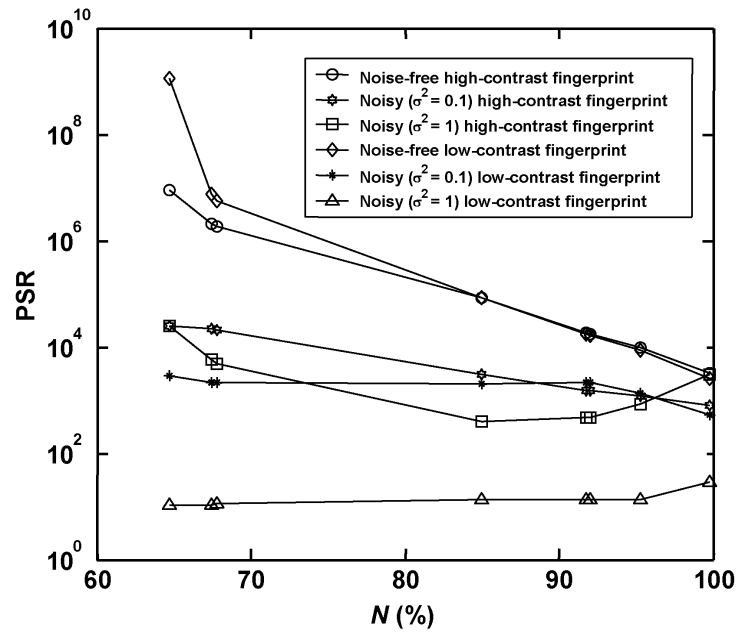
Figure 4.8 PSR as a function of the percentage N of low-contrast fingerprint reference.
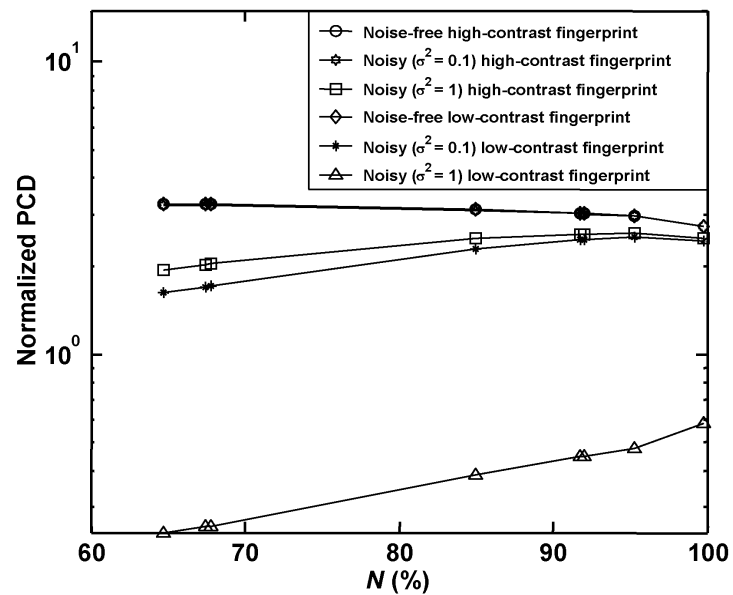
Figure 4.9 Normalized PCD of the primary peak as a function of the percentage N of low-contrast fingerprint reference.

4.3.3 High-contrast human face as the reference image

The 3-D plots of the correlation outputs of detecting noise-free and high-contrast targets are illustrated in Figs. 4.10(a) and 4.10(b) for the AMF with (a) $N =$ 96.3% that corresponds to low threshold and (b) $N = 99.9\%$ that corresponds to high threshold. Unlike the multiple-fingerprint detections, the secondary peak can be observed. This is because the power spectrum of the human face image concentrates at low-spatial frequencies. When the AMF generated by a high threshold is applied to the JPS, only a narrow band of low frequency components of the target and the unwanted target are attenuated. Thus the secondary peak is not suppressed efficiently. The full-area at half maximum of the primary peak of the human face image is about 132 pixels, which is broader than that of the fingerprint image because the human face image contains less high-spatial-frequency components. As predicted, the primary peak intensity is sharper and higher than the secondary peak, because the target matches the reference. Since the AMF with low threshold attenuates low-spatial-frequency components of the modified JPS more than that with high threshold, the primary peak of Fig. 4.10(a) is sharper and lower than that of Fig. 4.10(b), whereas its secondary peak is significantly degenerated. Consequently, this AMF causes the correlation plane of Fig. 4.10(a) to be less noisy than that of Fig. 4.10(b). Figures 4.10(c) and 4.10(d) show the correlation outputs of the noisy high-contrast targets with variance $\sigma^2 = 1$ pre-processed by the AMF with $N =$ (c) 96.3% and (d) 99.9%. In comparison with Figs. 4.10(a) and 4.10(b), the strong input noise causes a decrease in the primary peak intensities by about one order of magnitude and an increase in noise in the correlation plane.

Figures 4.11(a) and 4.11(b) present the 3-D plots of the correlation outputs of detecting noise-free and low-contrast targets obtained by using the AMF with $N =$ (a) 96.3% and (b) 99.9%. Their primary peaks reduce by about one order of magnitude as compared to Figs. 4.10(a) and 4.10(b), because the contrast ratio c_T which is smaller than unity scales the desired correlation. The reductions also occur on the secondary peaks. The correlation outputs of the noisy low-contrast targets with variance $\sigma^2 = 1$ are shown in Figs. 4.11(c) and 4.11(d) for the AMF with $N =$ (c) 96.3% and (d) 99.9%. In this case, the correlation peaks are degraded, because the luminance of the low-contrast target is smaller than the noise with variance $\sigma^2 = 1$ as discussed in previous work (Widjaja and Suripon, 2004). Thus, the noise in the correlation plane of Figs. 4.11(c) and 4.11(d) appears stronger than that of Figs. 4.10(c) and 4.10(d) even with the same noise level. When the AMF with low threshold is employed, the correlation peaks are further lowered. Therefore, the primary peak in Fig. 4.11(c) is indistinguishable from the noise.

Figure 4.12 shows the variation of the PSRs as a function of the percentage N for different targets detected by the high-contrast reference. In general, the PSRs are lower than those of the fingerprint detection. As discussed in the beginning of this section, this is attributed to the presence of the strong secondary peaks. In the case of the high-contrast targets, the PSRs become higher as the percentage N decreases, and the PSR increases faster for the noise-free target than for the noisy one. This is explained as follows. Firstly, the secondary peak which is lower than the primary peak is rapidly degenerated with decreasing N as shown in Fig. 4.10, since the AMF of low percentage N attenuates the power spectrum more strongly than that of high percentage N. Thus the difference between the primary and secondary peaks increases.

Secondly, in the case of the detection of the noisy targets, the primary peak is corrupted by the noise. Therefore, the PSR becomes the lowest as the noise variance becomes unity. In comparison with the high-contrast human face images, the detection of the low-contrast target gives different PSRs. In the case of the noise-free low-contrast target, the value of its PSR increases suddenly to be 23091 at $N = 99.2\%$. It is found that the corresponding AMF attenuates more low-frequency components of the JPS at this percentage than $N = 99.9\%$. This attenuation relatively enhances high-frequency components of the JPS. Since the high-frequency components of the unwanted target are totally different from those of the reference, the secondary peak is significantly degenerated. In contrast, the primary peak is sharpened, because its frequency components match those of the reference. When the percentage N reduces to 98.5%, the primary peak becomes lower, since the power spectrum at higher frequencies declines. Consequently, the PSRs decrease again. In the case of the noisy target with variance $\sigma^2 = 1$, the PSRs are less than unity for low values of N, because of the presence of the strong noise at the correlation plane.

The normalized PCDs of the primary peak of the modified AMJTC are shown in Fig. 4.13 as a function of percentage N. The PCD is greater than 1 in all the cases except for the noisy target with variance $\sigma^2 = 1$, where the strong noise appearing in the correlation plane degrades the primary peak and gives rise to PCD less than unity. These results are in agreement with the previous chapter. Therefore, in the case of the noisy low-contrast target with variance $\sigma^2 = 1$, the performance of multiple-target detection cannot be improved because its PSRs and normalized PCDs are less than unity. In contrast, the detection performance of the modified AMJTC of other cases can be done by using any threshold value.
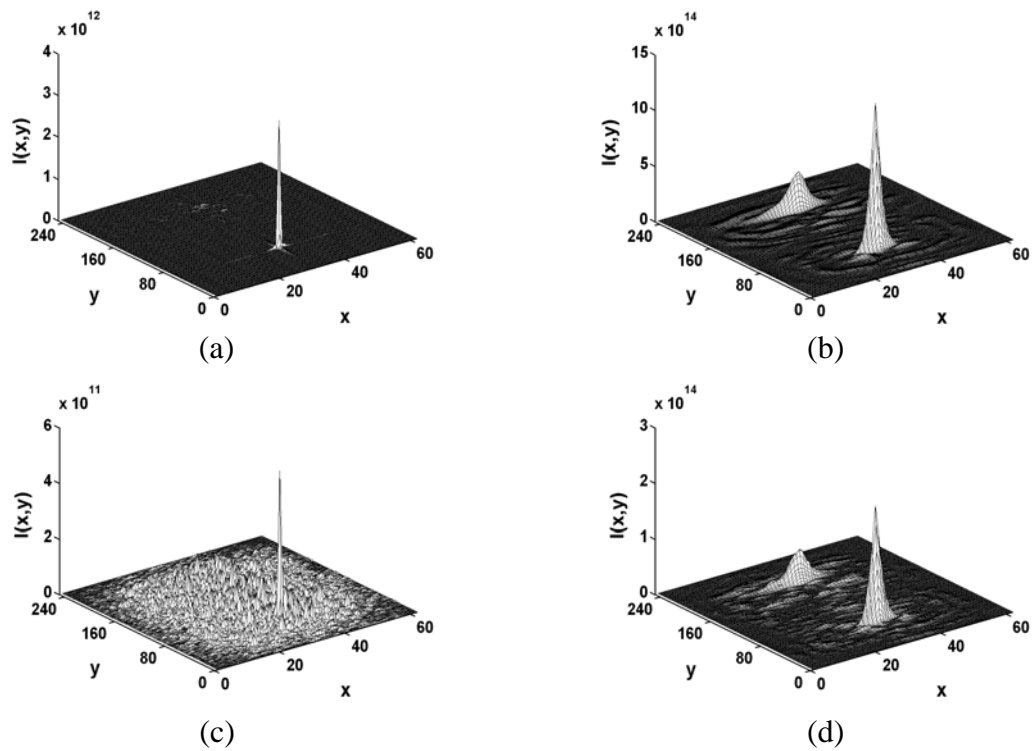
Figure 4.10 Correlation outputs of noise-free high-contrast multiple-human face detections pre-processed by the AMF with $N =$ (a) 96.3% and (b) 99.9%, and of noisy high-contrast target ($\sigma^2 = 1$) pre-processed by the AMF with $N =$ (c) 96.3% and (d) 99.9%.
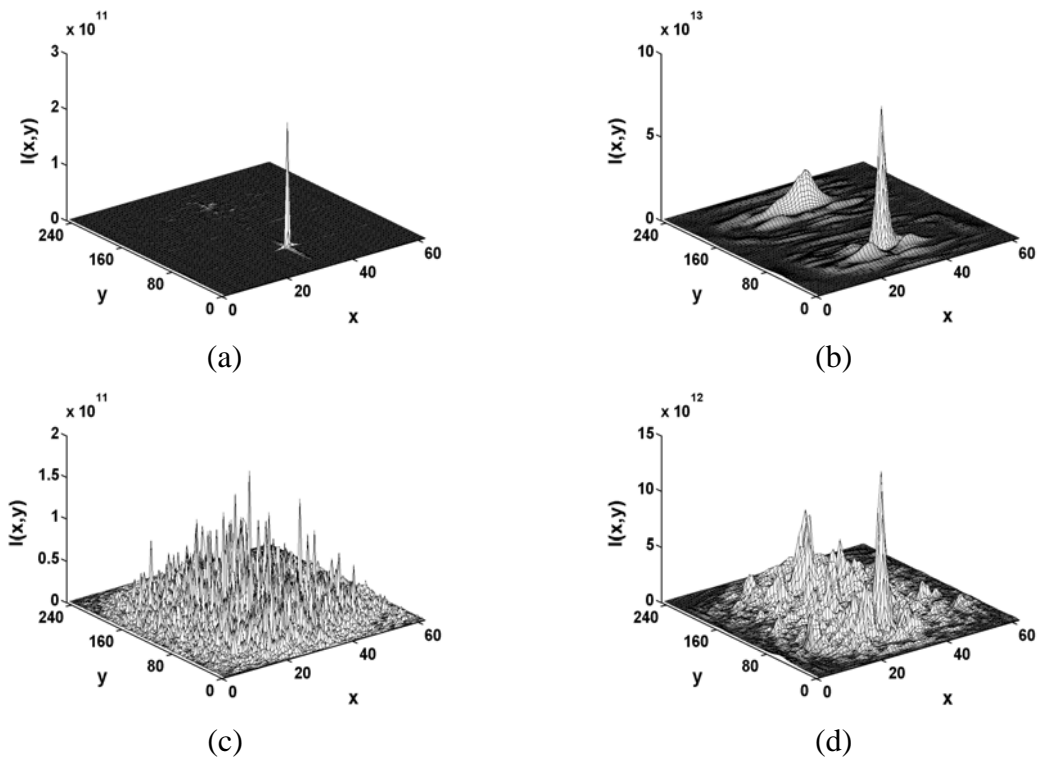
Figure 4.11   Correlation outputs of noise-free low-contrast multiple-human face detections pre-processed by the AMF with N = (a) 96.3% and (b) 99.9%, and of noisy low-contrast target ($\sigma^2 = 1$) pre-processed by the AMF with N = (c) 96.3% and (d) 99.9%.
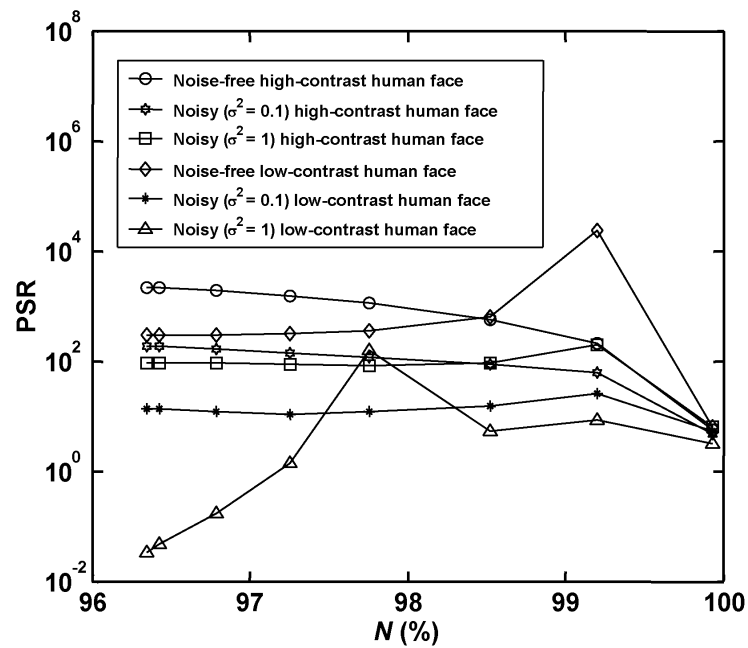
Figure 4.12 PSR as a function of the percentage N of high-contrast human face reference.
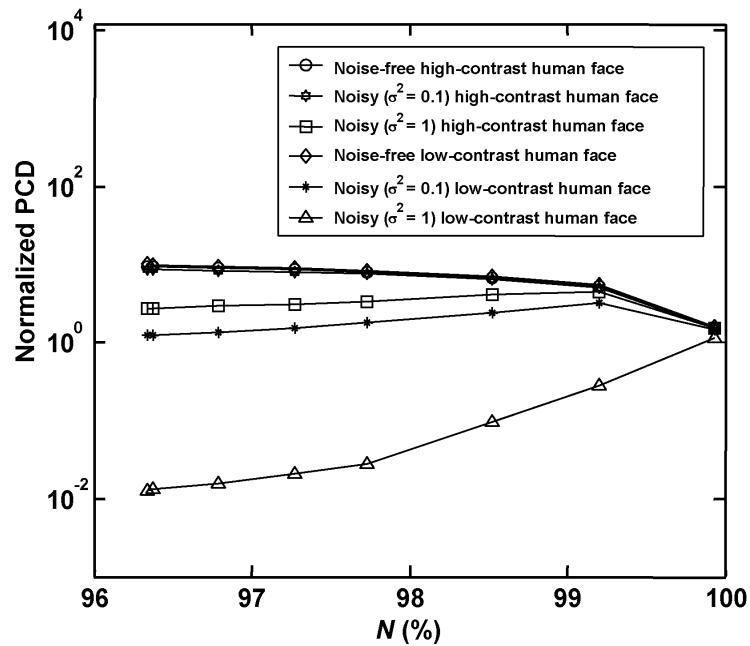
Figure 4.13 Normalized PCD of the primary peak as a function of the percentage N of high-contrast human face reference.

4.3.4 Low-contrast human face as the reference image

Figures 4.14(a) and 4.14(b) show the 3-D correlation outputs of detecting noise-free and low-contrast targets obtained by using the AMF with (a) N = 96.3% that corresponds to low threshold and (b) N = 99.9% that corresponds to high threshold. In comparison with Figs. 4.10(a) and 4.10(b), respectively, the correlation peaks are lower in intensity by about two orders of magnitude and broader in width. The differences in peak between Figs. 4.14(a) and 4.14(b) are caused by the AMF which is generated by the different threshold values. The correlation outputs of the noisy low-contrast targets with variance σ^2 = 1 are presented in Figs. 4.14(c) and 4.14(d) for the AMF with N = (c) 96.3% and (d) 99.9%. It is obvious that the primary peak of the Fig. 4.14(c) is buried in noise. This occurs because the correlation of the low-contrast reference and the noise can be greater incidentally in some portions than that of the low-contrast target and the reference.

Figures 4.15(a) and 4.15(b) illustrate the correlation outputs of detecting noise-free and high-contrast targets pre-processed by the AMF with N = (a) 96.3% and (b) 99.9%, while the results for the noisy high-contrast targets with variance σ^2 = 1 are shown in Figs. 4.15(c) and 4.15(d) for the same AMF as Figs. 4.15(a) and 4.15(b), respectively. Since the target contrast is high, the correlation peaks of these figures are higher than those of Figs. 4.14(a) – (d), respectively. It is obvious that the primary peaks in Fig. 4.15(c) can be clearly detected.

Figures 4.16 and 4.17 show the PSRs and the normalized PCDs of the low-contrast references as a function of the percentage N, respectively. They are similar to those of the high-contrast references, because their correlation intensities are decreased by the same scale. As the case of the fingerprint detections, the detection

performance of the modified AMJTC depends on the contrast of the human face target.
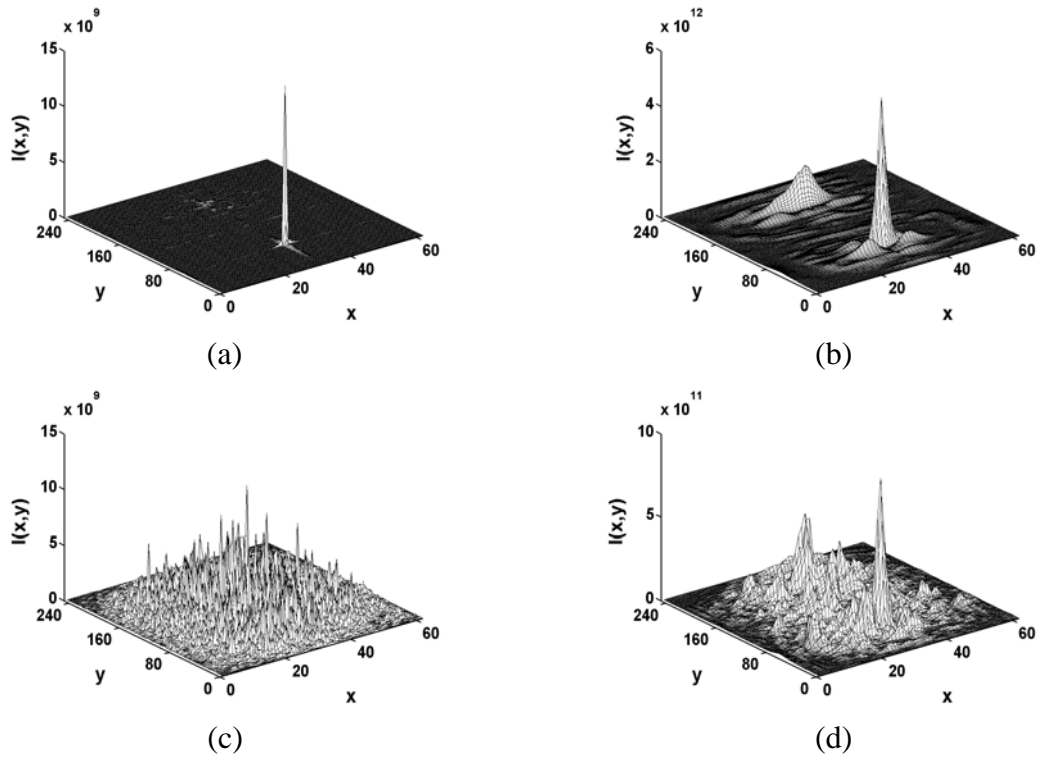
Figure 4.14   Correlation outputs of noise-free low-contrast multiple-human face detections pre-processed by the AMF with N = (a) 96.3% and (b) 99.9%, and of noisy low-contrast target ($\sigma^2 = 1$) pre-processed by the AMF with N = (c) 96.3% and N = (d) 99.9%.
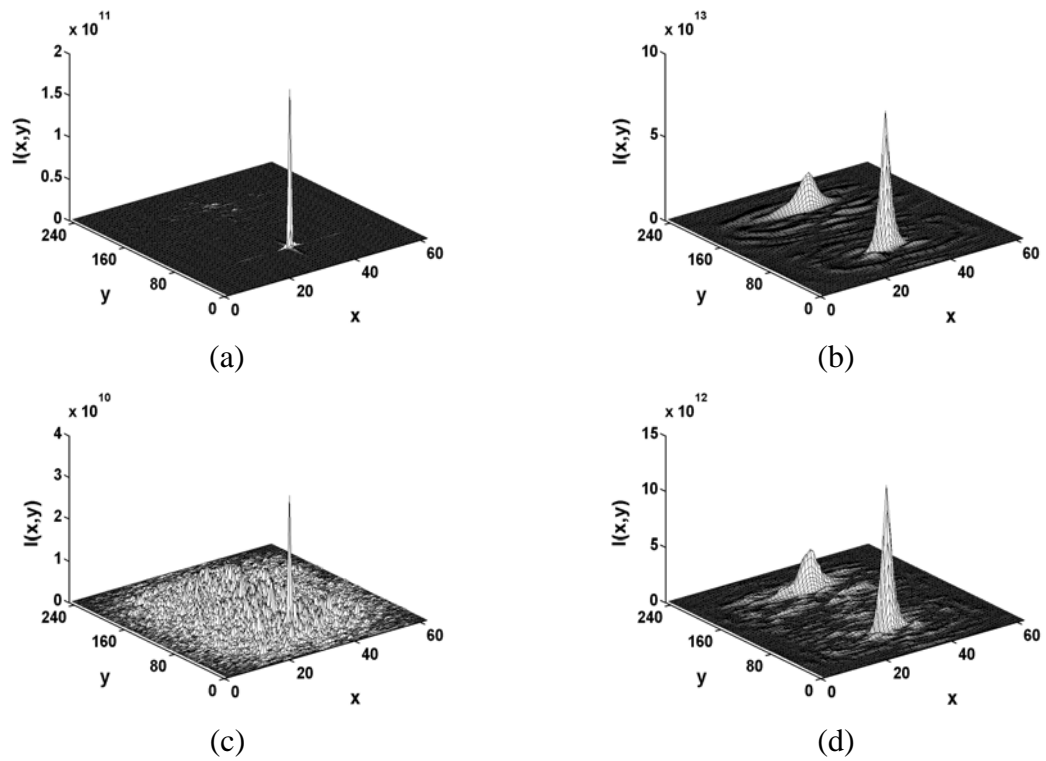
Figure 4.15 Correlation outputs of noise-free high-contrast multiple-human face detections pre-processed by the AMF with N = (a) 96.3% and (b) 99.9%, and of noisy high-contrast target ($\sigma^2 = 1$) pre-processed by the AMF with N = (c) 96.3% and (d) 99.9%.
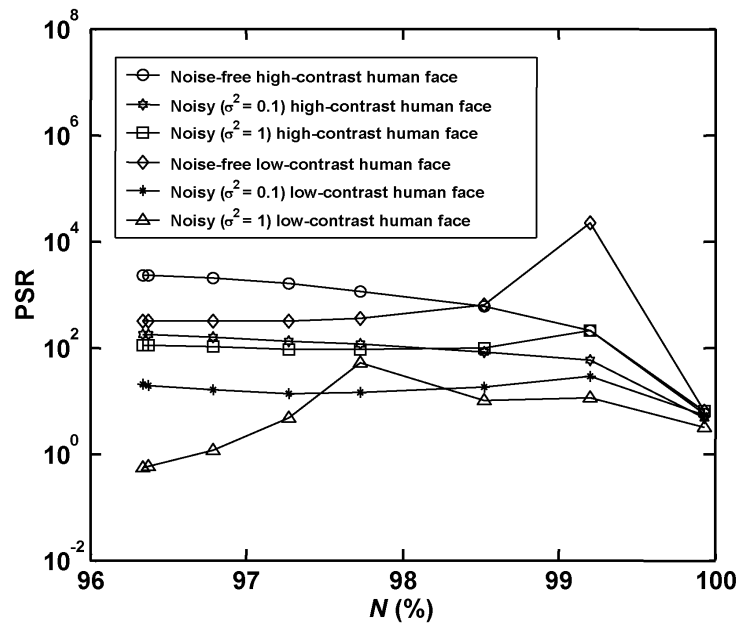
Figure 4.16   PSR as a function of the percentage N of low-contrast human face
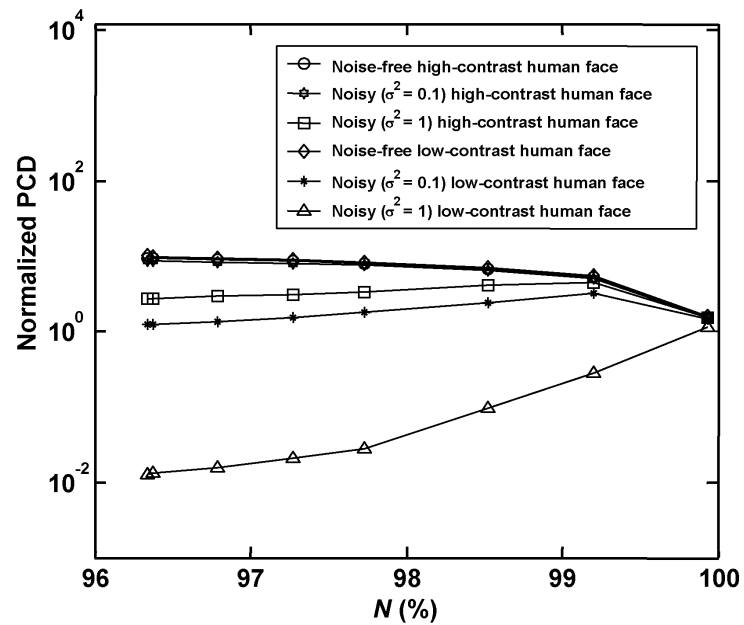
reference.

**Figure 4.17**   Normalized PCD of the primary peak as a function of the percentage N

of low-contrast human face reference.

Considering that the PSR should be as high as possible and that the normalized PCD should be greater than unity, the detection performance can be optimized by selecting appropriate threshold value as in Table 4.1. Regardless of the spatial-frequency contents of the high-contrast targets, and of the level of the noise presence, the performance of the modified AMJTC can be optimized by using the AMF synthesized with low threshold value The detection of the low-contrast image with high spatial-frequency contents can also be maximized by using the AMF with low-threshold value. For the low-contrast image with low spatial-frequency content, however, intermediate threshold should be used and the modified AMJTC fails to detect any noise corrupted low-contrast images.

Table 4.1 Optimization condition for multiple-target detection by using the modified AMJTC

Reference images	Condition for target images			
	Noise free		Noisy	
	High contrast	Low contrast	High contrast	Low contrast
High-contrast fingerprint	Low threshold	Low threshold	Low threshold	None
Low-contrast fingerprint	Low threshold	Low threshold	Low threshold	None
High-contrast human face	Low threshold	Intermediate threshold	Low threshold	None
Low-contrast human face	Low threshold	Intermediate threshold	Low threshold	None

CHAPTER V

TARGET DETECTION USING SMOOTHED

AMPLITUDE-MODULATED FILTER

As shown in the previous chapters, the detection performance of the modified AMJTC is determined by the selected threshold value which depends on a noise level, a contrast and a spatial-frequency content of an input target image. For an intra-class target recognition, a set of AMFs may be required. In order to reduce dependence of the detection performance on a threshold value, a new method for improving detection performance of modified AMJTC by smoothing the AMF is proposed in this chapter. The studies are investigated by using computer simulation. To compare the effect of threshold on single- and multiple-target detection using smoothed AMF with the original AMF, the same test scenes and performance matrices are used.

5.1 Smoothed amplitude-modulated filter

The dependence of the detection performance on the selected threshold value can be explained by using Fig. 2.4. It is apparent that regardless of the threshold value, the AMF contains several cutoff frequencies. This is because several frequency components of the reference image can satisfy the second condition of Eq. (2.5). Since the AMF has a set of passbands and its transfer function is a non-smooth function, the threshold value affects the detection performance of the modified AMJTC. For the intra-class pattern recognition, the modified AMJTC may require a set of AMFs, which is impractical. For this reason, the smoothed AMF is proposed to improve the

detection performance of the modified AMJTC. To smooth the generated AMF, the following steps are taken:

1. Set the dc frequency and its neighbourhood to be zero.

2. Start with the filter response in the horizontal direction.

3. Separate the frequency response into positive and negative parts.

4. For each part, search for a cutoff frequency that is the nearest frequency component to the dc frequency and has a unity amplitude.

5. Set amplitude of all frequency components higher than the cutoff frequency to be unity. This is the step where the unwanted passbands are eliminated.

6. For lower ones, the amplitude of the low frequency component f_n must be smaller or equal to that of the higher component f_{n+1}. If this condition is not satisfied by the frequency f_n, the first lower frequency component f_k having lower amplitude than that of f_{n+1} is searched. The amplitude of the frequency components between f_k and f_{n+1} is determined by a linear interpolation. This process is stop when amplitude of f_k = 0.

7. Repeat the steps 4-6 for every row of the positive and the negative frequency components.

8. Store the resultant filter response into a new array.

9. Repeat the steps 2-8 for the vertical frequency components.

5.2 Computer simulation

In order to compare with our previous chapters, the same fingerprint and human face images were used as test scenes. Since the previous studies found that the contrast of the reference image does not affect the detection performance, only high-contrast images were used as the reference. To compare the detection performance of

the original AMF and the smoothed AMF, the modified JPS was digitally multiplied with the smoothed filter.

Figures 5.1(a) and 5.1(b) show the 3D-plot of the resultant transfer function obtained by smoothing the AMFs of fingerprint shown in Figs. 2.4 and 2.5, respectively. While, Figs. 5.2(a) and 5.2(b) show the 3D-plot of the resultant transfer function obtained by smoothing the AMFs of human face shown in Figs. 2.6 and 2.7, respectively. It is obvious that the smoothed AMF becomes a highpass filter whose bandwidth is determined by the threshold. The low threshold gives higher cutoff frequency than the high threshold does. By calculating the inverse Fourier transform of the product of the modified JPS and the smoothed AMF, and then taking the square modulus of the result, the correlation peak intensity was obtained as the final result. In the case of single-target detection, the PCD are used to measure the quality of the correlation output, while for multiple-target detection, the PSR are used to measure the discrimination ability of the correlation output.

(a)

(b)
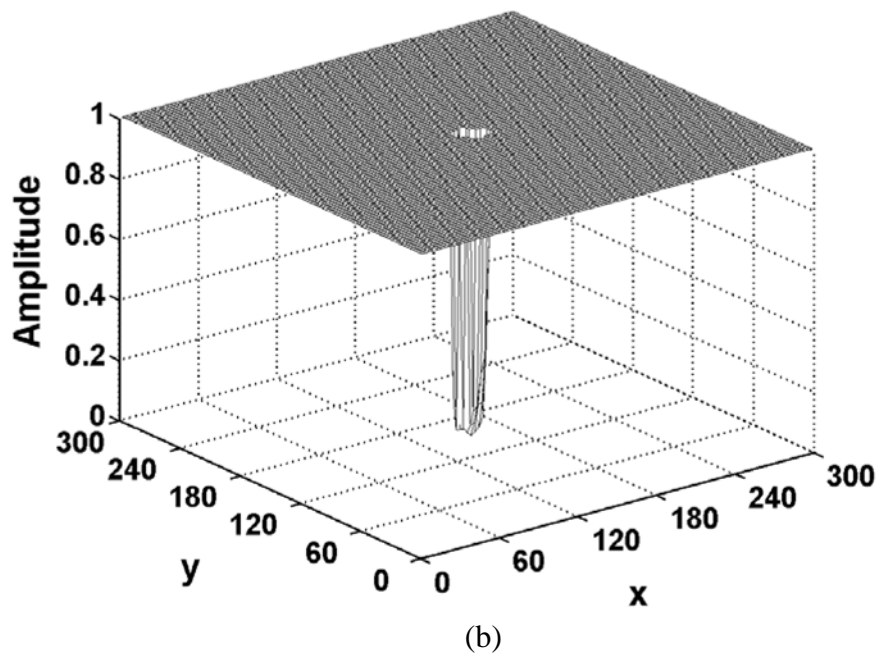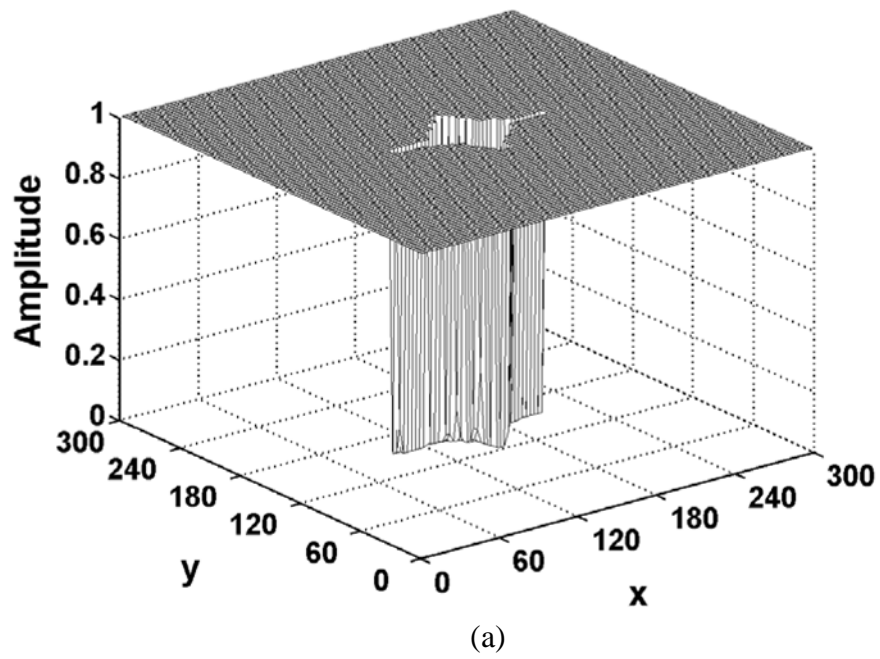
Figure 5.1 3-D plots of the resultant transfer function obtained by smoothing the AMFs generated from the fingerprint reference by using (a) low threshold and (b) high threshold.
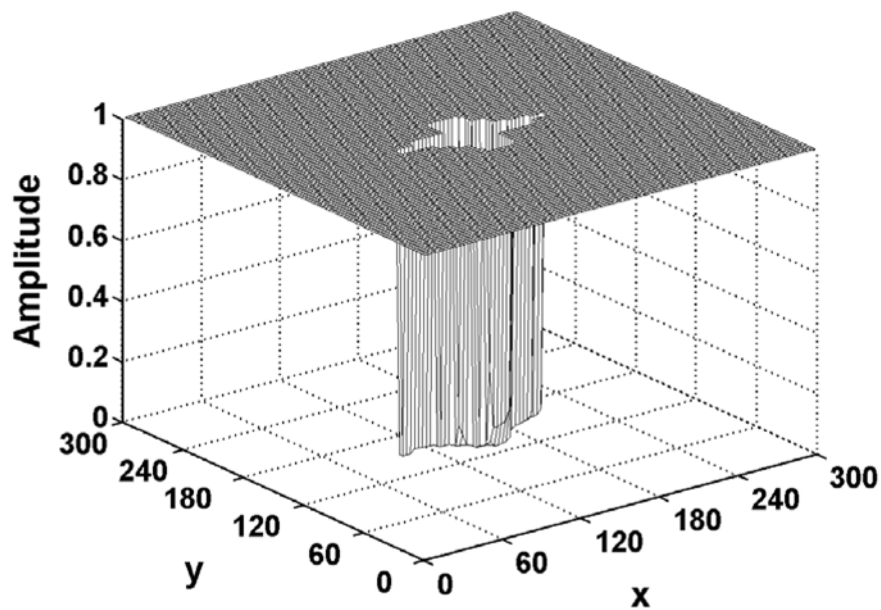
(a)
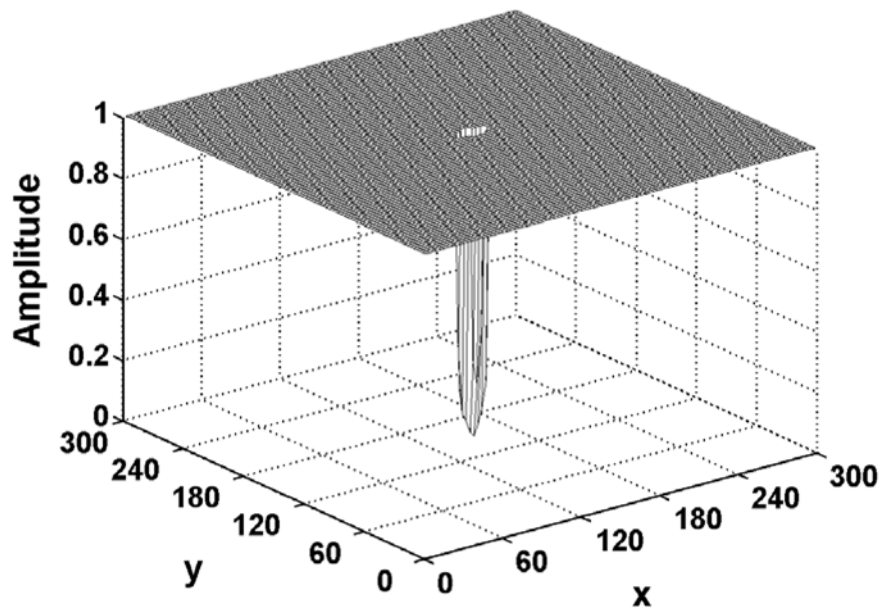
(b)

Figure 5.2 3-D plots of the resultant transfer function obtained by smoothing the AMFs generated from the human face reference by using (a) low threshold and (b) high threshold.

5.3 Simulation results

5.3.1 Single-target detection

5.3.1.1 Fingerprint as the reference image

The normalized PCDs of the modified AMJTC produced by using the conventional and the smoothed AMFs as a function of the percentage N for different target scenes are shown in Fig. 5.3. They are represented by using the broken and the solid lines, respectively. Regardless of the target contrast, the normalized PCDs of the noise-free fingerprint targets obtained by using the smoothed AMF are lower than those by the original AMF. This is because the smoothed AMF does not attenuate most low-spatial-frequency components of the JPS. As a correlation intensity is higher than that of the conventional AMF, the standard deviation is also higher. On the other hand, by smoothing the AMF the stopband of the filter generated by the low threshold does not differ significantly from that by the high threshold. As a consequence, although their PCDs at the low percentage $N = 66.7\%$ are optimized, it is only slightly different from those at $N = 99.8\%$. For the same reason, the dependence of the noisy high-contrast fingerprint detections on the threshold value can be reduced by smoothing the AMF. In the case of the noisy low-contrast target, only when the noise variance $\sigma^2 = 1$, the normalized PCD never exceeds unity. Therefore, no improvement of the detection is achieved. In addition, a full-area at half maximum of the correlation peak is always equal to 1×1 pixel. This shows that the correlation width is not affected by the use of the smoothed AMF. In summary, since almost all PCDs are maximized at the low percentage N, a single smoothed AMF generated at a low threshold can be used for recognition of intra-target scenes, regardless their contrast and noise.
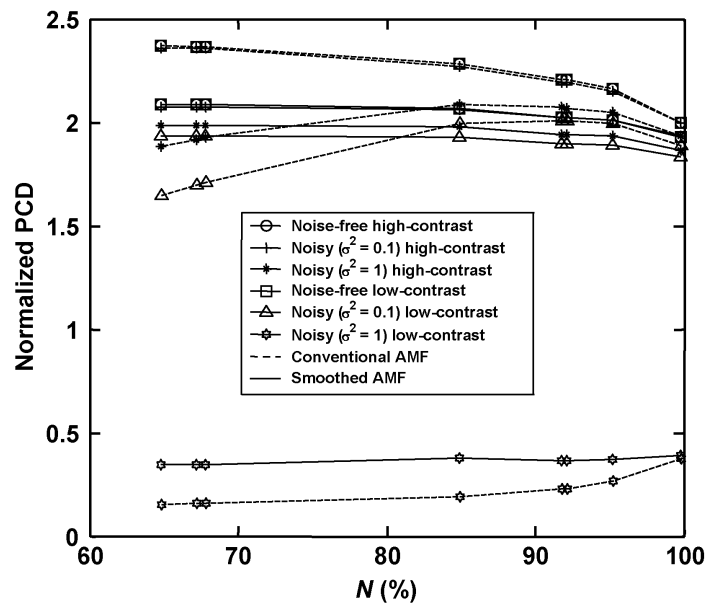
Figure 5.3 The normalized PCD as a function of the percentage N of fingerprint reference produced by the conventional and the smoothed AMFs.

5.3.1.2 Human face as the reference image

Figure 5.4 illustrates the variation of normalized PCDs produced by the conventional and the smoothed AMFs as a function of the percentage N for different target scenes. They are also represented by the broken and the solid lines, respectively. In comparison with the fingerprint detections, the normalized PCDs of the human face generated by the smoothed AMF increase faster as the percentage N becomes smaller. This is caused by the fact that human face images contain mainly low spatial-frequency components. Consequently, its corresponding JPS is easily modified by a small change of the stopband of the smoothed AMF. For the same reason as discussed in Sect. 5.3.1.1, the PCDs of the noise-free human face targets produced by the smoothed AMF are lower than that by the conventional one. The advantage of smoothing the AMF can also be observed from the resultant detections of the noisy

high- and low-contrast targets which can be optimized by a single smoothed AMF generated at low threshold. Note that the detection of the low-contrast target corrupted by the noise with variance $\sigma^2 = 1$ should be done with caution, because the smoothed AMF generated at the highest threshold may also produce high PCD. Finally, although the smoothed AMF gives a greater full-area at half maximum than the conventional AMF does, its variation in respect to the percentage N has the same tendency. Therefore, the optimization condition is determined solely by the PCD.
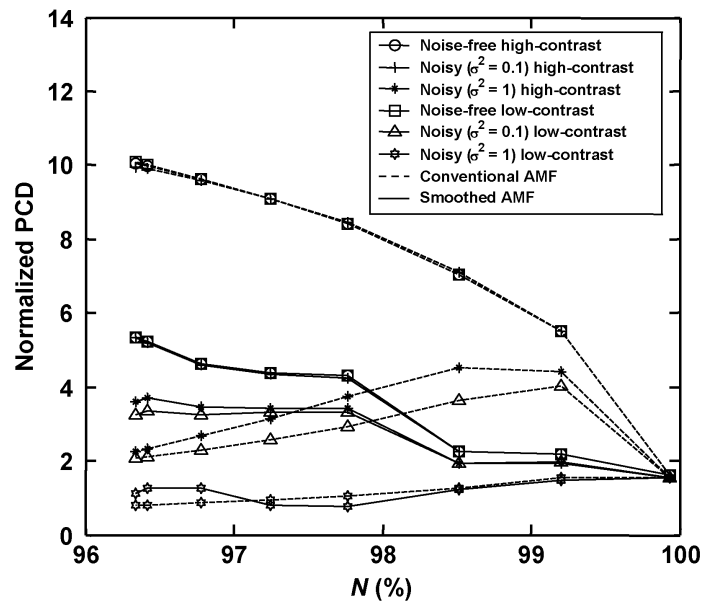

Figure 5.4 The normalized PCD as a function of the percentage N of human face reference produced by the conventional and the smoothed AMFs.
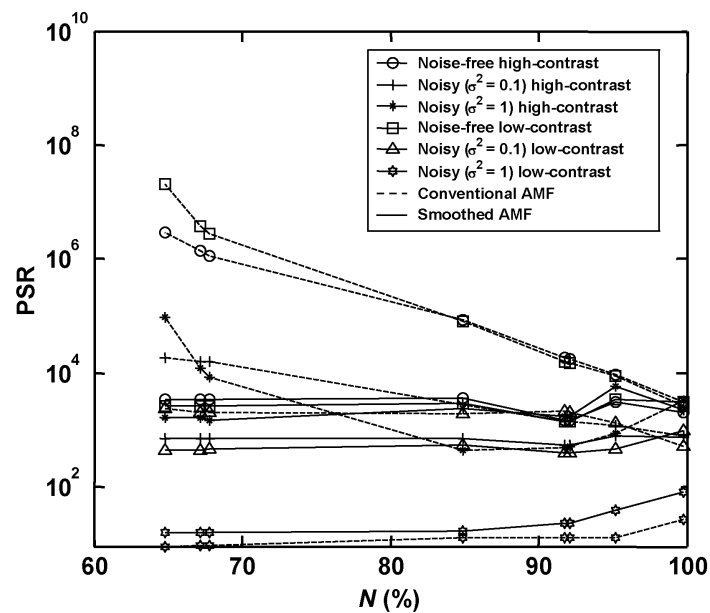
5.3.2 Multiple-target detection

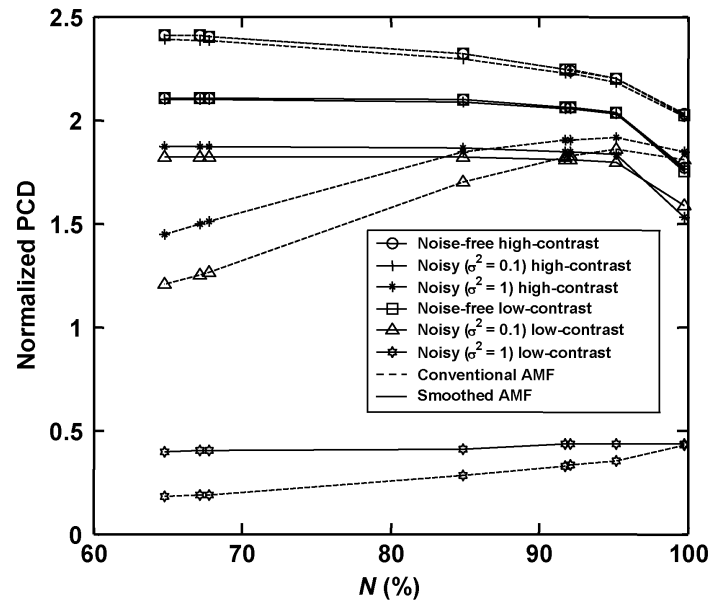#### 5.3.2.1 Fingerprint as the reference image

The PSRs of the modified AMJTC produced by the conventional and the smoothed AMFs of high-contrast fingerprint reference as a function of the percentage N for different target scenes are shown in Fig. 5.5 by using the broken and the solid lines, respectively. Although almost all cases of the detection using the smoothed AMF give the PSRs lower than using the conventional AMF but their PSRs are still greater than 400. Only in the case of the noisy low-contrast target detection with variance $\sigma^2 = 1$, the PSR of the detection using the smoothed AMF is about 20. It is higher compared with the noisy low-contrast target detection using the conventional AMF, because the detection using the smoothed AMF produces higher primary peak and lower secondary peak. When the thresholds are varied, the PSRs produced by using the smoothed AMF do not change because the stopband of the smoothed AMF generated by different thresholds are not vary drastically. For high-contrast target detection, the PSR of the noisy target with variance $\sigma^2 = 1$ is higher than that of the noisy target with variance $\sigma^2 = 0.1$. This is because the secondary peak of the noisy high-contrast target with variance $\sigma^2 = 1$ is reduced much more than that of the noisy high-contrast target with variance $\sigma^2 = 0.1$. For low-contrast target detection, their PSRs decrease depending on the noise level of the target.

Figure 5.6 presents the normalized PCDs of the primary peak as a function of the percentage N for different target scenes. Like the single-target detection, the normalized PCDs of noise-free high- and low-contrast multiple-fingerprint target detection using the smoothed AMF are also lower than that of the detection using the conventional AMF. In the case of noisy low-contrast target with variance $\sigma^2 = 1$, the

normalized PCD produced by using the smoothed AMF is higher than that of the detection using the conventional AMF because the smoothed AMF attenuates less high-spatial-frequency components. For all cases, their PCDs generated by low threshold are also not much different from that of high threshold. This is because the stopband of the smoothed AMF does not change drastically. By considering the PSR and the normalized PCD of the primary peak, the detection performance of the modified AMF obtained by using the smoothed AMF can be optimized by using single threshold value except in the case of noisy low-contrast target detection with variance $\sigma^2 = 1$ since its normalized PCD is less than unity.

Figure 5.5 The PSR as a function of the percentage N of fingerprint reference produced by the conventional and the smoothed AMFs.

Figure 5.6 The normalized PCD as a function of the percentage N of fingerprint reference produced by the conventional and the smoothed AMFs.

5.3.2.2 Human face as the reference image

Figure 5.7 shows the variation of the PSRs generated by using the conventional and the smoothed AMFs of high-contrast human face reference as a function of the percentage N for different target scenes. The broken and the solid lines correspond to the PSRs produced by using the conventional and the smoothed AMFs, respectively. Unlike using conventional AMFs, all PSRs obtained by using the smoothed AMF are higher than 5. In the case of noise-free high-contrast target, the detection of the modified AMJTC generated by using the smoothed AMF gives lower PSR compared to that by using the conventional AMF. This is because the smoothed AMF attenuates more low-spatial-frequency components than the conventional AMF and the human face images contain mainly low spatial-frequency components. In the case of noisy high-contrast target, the detection by using the smoothed AMF generates

the higher PSR compared to that by using the conventional AMF. For the low-contrast target detection, the PSR produced by using the smoothed AMF is higher than that by using the conventional AMF and at low threshold value, the PSRs decrease depended on the noise level of the target.

The normalized PCDs of the primary peak as a function of the percentage N for different target scenes are illustrated in Fig. 5.8. Similarly to the single-target detection, the normalized PCDs of multiple-human face detection obtained by using the smoothed AMF are higher compare to that of multiple-fingerprint detection. For noise-free high- and low-contrast target detection, the normalized PCDs of the modified AMJTC generated by using the smoothed AMF are lower than that by using the conventional AMF, while at low threshold the normalized PCDs of noisy target detection produced by using the smoothed AMF are higher than that by using the conventional AMF. Thus, the detection performance of noisy multiple-human face detection can be optimized by selecting low threshold value. However, the noisy low-contrast target detection with variance $\sigma^2 = 1$ may fail to improve the detection performance since its normalized PCD is less than unity.

Figure 5.7   The PSR as a function of the percentage N of human face reference produced by the conventional and the smoothed AMFs.
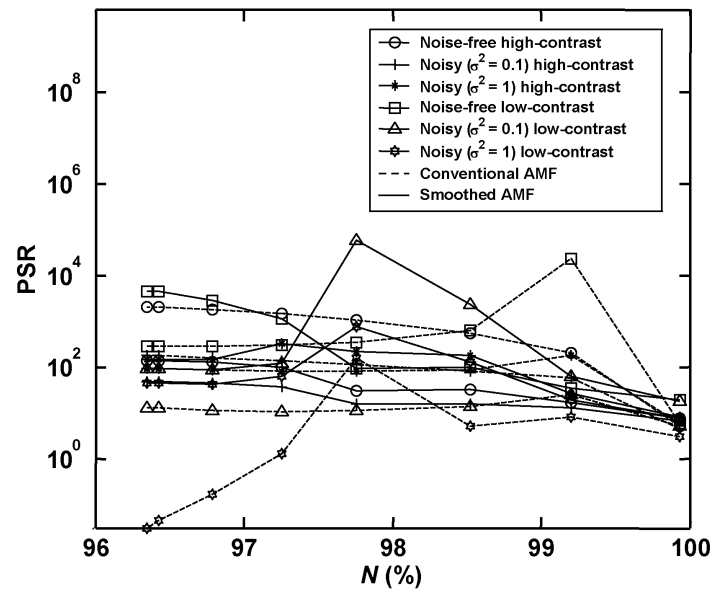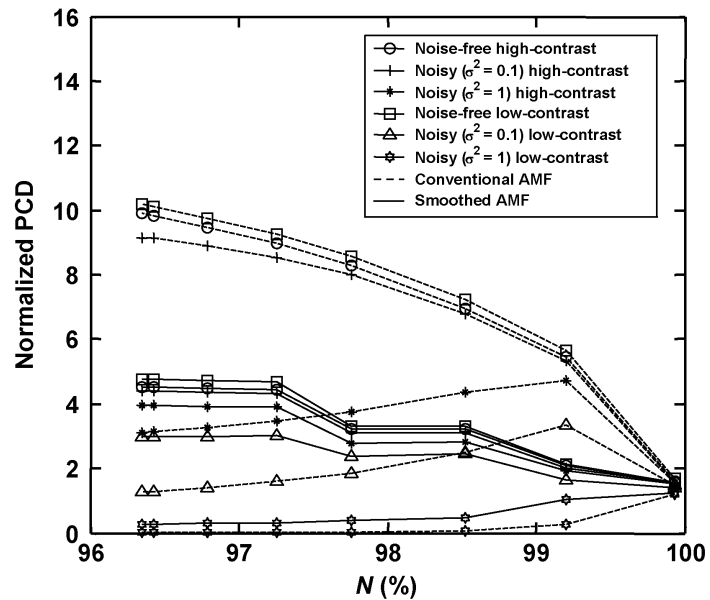

Figure 5.8   The normalized PCD as a function of the percentage N of human face reference produced by the conventional and the smoothed AMFs.

CHAPTER VI

CONCLUSIONS

This dissertation investigated the optimization performance of the target detection using the modified AMJTC. To conduct this investigation, the first part of this dissertation addressed the effects of the threshold on the detection performance, whereas the second part proposed the improvement of the modified AMJTC by smoothing the AMF. The studies of single- and multiple- targets were performed by using the computer simulation with Matlab 6.0 run on a Windows-based personal computer. The fingerprint and the human face images were used as test scenes having different spatial-frequency contents. The studies considered the presence of noise in the input plane and a contrast difference between the target and the reference images that may arise from unbalanced illumination.

In Chapter II, the standard architecture of a joint transform correlation was briefly reviewed. The discussion was followed with the architecture of the modified AMJTC.

In Chapter III, the effects of threshold on single-target detection of the modified AMJTC were investigated by using the PCD and the FAHM. Of the four types of reference images, the normalized PCD of the human face detection is greater than that of the fingerprint. This is because broad correlation peak produced by the classical JTC yields smaller value of the PCD of the human face detection compared to the fingerprint. When the PCD of the human face detected by the modified AMJTC is normalized by the resultant classical PCD, its normalized PCD becomes larger than

that of the fingerprint. By taking the value of normalized PCDs into account, the simulation results show that the detection of human face can be improved greater than that of fingerprint. The effects of threshold on single-target detection depend on the noise level in the input, the contrast and the spatial-frequency content of the target. When the target is low-contrast image with high-spatial frequency content, the modified AMJTC is not tolerant to noise.

The effects of threshold on detection performance of multiple targets by using the modified AMJTC was discussed in Chapter IV. As shown in Chapter III that the performance of the single-target detection using the modified AMJTC can be optimized by selecting appropriate threshold value. In general, the input scenes may consist of wanted and unwanted targets. Thus, a study of multiple-target detection performance using the modified AMJTC is important. By taking this into account, in this chapter we investigate quantitatively the effects of threshold on detection performance of multiple targets by using the modified AMJTC by means of the computer simulation. In this work, the fingerprint and the human face images with different contrast and in the presence of noise were used as test scenes. The detection performance was quantitatively measured by using the PSR and the normalized PCD of the primary peak. The simulation results show that the PSR of the detection of the fingerprint is higher than that of the human face. Detections of the both types of images depend on the contrast of the target. Regardless of the spatial-frequency contents of the high-contrast targets, and of the level of the noise presence, the performance of the modified AMJTC can be optimized by using the AMF synthesized with low threshold value. The detection of the low-contrast image with high spatial-frequency contents can also be maximized by using the AMF with low-threshold

value. For the low-contrast image with low spatial-frequency content, however, intermediate threshold should be used. This may be caused by the fact that this image has the lowest spatial-frequency content. Finally, the modified AMJTC fails to detect any noise corrupted low-contrast images.

In Chapter V, a novel method for improving the detection performance of the modified AMJTC by smoothing the AMF was proposed. The simulation results show that a single smoothed AMF generated at a low threshold can be used for optimizing recognitions of intra-target scenes, regardless the contrast, noise and the spatial-frequency content of the target images. In comparison with conventional AMF, this proposed method may simplify implementation of the real-time modified AMJTC, because it requires less storage for storing filters. In the case of multiple-target detection, only the detection performance of high-spatial-frequency content of the target images can be optimized using a single smoothed AMF generated at low threshold.

REFERENCES

REFERENCES

Alam, M.S. and Karim, M.A. (1993). Fringe-adjusted joint transform correlation. **Applied Optics.** 32(23): 4344-4350.

Alam, M.S. and Karim, M.A. (1994). Multiple target detection using a modified fringe-adjusted joint transform correlator. **Optical Engineering.** 33(5): 1610-1617.

Antoine, J., Vandergheynst, P., Bouyoucef, K. and Murenzi, R. (1995). Target detection and recognition using two-dimensional isotropic and anisotropic wavelets. **Proceedings of the SPIE International Society of Optical Engineering: Automatic Object Recognition V.** July, 2485: 20-31.

Feng, D., Zhao, H. and Xia, S. (1991). Amplitude-modulated JTC for improving correlation discrimination. **Optics Communications.** 86(3-4): 260-264.

Goodman, J.W. (1996). **Introduction to Fourier optics** (2nd ed.). New York: McGraw-Hill.

Huang, X., Lai, H. and Gao, Z. (1997). Multiple-target detection with use of a modified amplitude-modulated joint transform correlator. **Applied Optics.** 36(35): 9198-9204.

Khan, J.F. and Alam M.S. (2005). Target detection in cluttered forward-looking infrared imagery. **Optical Engineering.** 44(7): 076404(1-9).

Liu, W., Kim, H., Lee S. and Lee, S. (1998). Joint transform correlator for the detection of defects in optical fibers. **Optical Engineering.** 37(5): 1468-1474.

Mallik B. and Datta A.K. (1999). Defect Detection in Fabrics with a Joint Transform Correlation Technique: Theoretical Basis and Simulation. **Textile Research Journal.** 69: 829-835.

Roberge, D. and Sheng, Y. (1994). Optical wavelet matched filter. **Optical Engineering.** 33(7): 2290-2295.

Widjaja, J. (1998). Automatic holographic particle sizing using wavelet-based joint transform correlator. **Optik.** 107(3): 132-134.

Widjaja, J. and Suripon, U. (2004). Real-time joint transform correlator using compressed reference image. **Optical Engineering.** 43(8): 1737-1745.

Widjaja, J. and Suripon, U. (2005). Multiple-target detection by using joint transform correlator with compressed reference images. **Optics Communications.** 253: 44-55.

CURRICULUM VITAE

Mrs. Pitchaya Kaewkasi was born on Febuary 22, 1979 in Nakhon Si Thammarat. She graduated with a B.Eng. degree, second-class honor, in computer engineering from Suranaree University of Technology, Thailand, in 2000 and she received her MCompSc degree in computer science from University of Wollongong, Australia, in 2002 and a M.S. degree in computer science from Kasetsart University, Thailand, in 2003. She pursuded her Ph.D. degree in laser technology at the School of Laser Technology and Photonics, Suranaree University of Technology, Thailand. Her research interests are in optical and digital image processing.